EXPERIMENTAL STUDY OF THE SHEAR ALFVEN

RESONANCE IN A TOKAMAK

by

FRANKLIN DOUGLAS WITHERSPOON

A thesis submitted in partial fulfillment of the

requirements for the degree of

Doctor of Philosophy

(Physics)

at the

UNIVERSITY OF WISCONSIN-MADISON

1984

ABSTRACT

EXPERIMENTAL STUDY OF THE SHEAR ALFVEN

RESONANCE IN A TOKAMAK

Franklin Douglas Witherspoon

Under the supervision of Professor Julien Clinton Sprott

Studies of a new rf heating technique in tokamaks, Shear Alfvén Resonance Heating, have been performed on the Tokapole II tokamak at the University of Wisconsin. High power heating experiments have been preceded by careful identification of the resonance and its properties at low power.

According to MHD theory, the shear Alfvén resonance manifests itself as a resonant enhancement of the wave magnetic field perpendicular to the equilibrium field at the location in the non-uniform plasma where the frequency, ω, and parallel wavelength match the Alfvén speed v_A, i.e. $\omega = k_{\parallel} v_A$. Experiments on the Tokapole II device have demonstrated the existence of the shear Alfvén resonance in a tokamak by direct probe measurement of the wave magnetic field within the plasma. The resonance is experimentally identified as a radially localized enhancement of the poloidal wave magnetic field. The radial location of the resonance agrees with a 2-D MHD

calculation which includes toroidicity and non-circularity of the plasma cross-section. Other properties of the resonance such as polarization, radial width, risetime to saturation, and resonant enhancement over the driving vacuum rf fields are found to be in good agreement with theory.

The resonances are driven by a novel launching structure which utilizes the four existing poloidal divertor rings within the vacuum vessel of Tokapole II. RF currents at ~1.2 MHz are driven through the mechanical supports of the divertor rings, and are superposed upon the transformer-induced equilibrium field shaping currents. Proper phasing of the currents in each ring allow approximation to poloidal mode numbers of m=1,2, or 4, and the toroidal structure of the antenna currents yields a step-wise approximation to toroidal mode numbers n=1 and 2. However, a broad n and m spectrum is generated.

These studies have provided the experimental base from which high power heating experiments utilizing the shear Alfvén resonance can be pursued.

Julian Clinton Sprott

MAY 3 1 1984

ACKNOWLEDGEMENTS

I would like to thank Professors J.C. Sprott and S.C. Prager for the support and advice they have given me throughout my graduate studies. I have also benefited from numerous discussions with Dr. C.E. Kieras and Professor J.A. Tataronis on the theoretical aspects of shear Alfvén heating of tokamaks. I especially want to thank Dr. Kieras for developing the numerical code which calculates the shear Alfvén resonance location in Tokapole II. I also would like to acknowledge the helpful advice and friendship of Professor R. Dexter.

A very special thanks goes to T. Lovell who kept Tokapole II going and without whose infinite patience and understanding this research would not have been possible. Special thanks also goes to my fellow graduate student D. Kortbawi who spent many a late night and weekend assisting in all facets of the experiment and who built, or assisted in building, much of the hardware. I wish him the best of luck in the future as he carries on with the experiment.

I have enjoyed working with all the graduate students in the UW plasma group but especially wish to thank the members of the Tokapole II group for their friendship and advice through the years: T. Osborne, D. Shepard, N. Brickhouse, A. Biddle,

D. Holly, T. Rempel, T. Leonard, M. Sengstacke and all the others.

I would also like to thank my parents Frank and Joyce Witherspoon and my brothers and sisters for their faith and support through the years.

Thanks go to my roommate and close friend of many years, Dr. Kevin Miller, and very special thanks go to my faithful dog Dora, who has put up with a lot of inattention and many late nights and yet still greeted me joyfully every time I returned home. She has been a joy in my life.

Last, but certainly not least, I wish to thank my fiancee, Margaret Daube, whose love and support over the past two years have kept me going when things were roughest.

Financial support was provided by the United States Department of Energy.

TABLE OF CONTENTS

CHAPTER 1

INTRODUCTION

It is sometimes the case that the dispersion relation which describes propagating waves in a uniform plasma, such as electrostatic plasma waves[1] or shear Alfvén waves[2], becomes a condition for a local resonance in a nonuniform plasma. If it can be arranged for an external antenna to match the mode structure and frequency of this resonance, then it may be possible to couple electromagnetic energy to the plasma from an external power source.

This theoretical result has been the cause of intensive research in the plasma physics community for many years. There are two primary reasons for this interest. First is the desire to understand the basic physics of the plasma state, for which waves are of fundamental importance. And secondly is the worldwide effort to produce a controlled fusion reactor.

The device which has received the most attention, and which is generally considered the closest to realization as a reactor, is the tokamak[3,4,5]. Like most other magnetic confinement devices, the basic tokamak design cannot reach ignition conditions on its own, but must rely on some form of auxiliary heating to supplement the ohmic heating of the toroidal current. Ohmic heating is insufficient because the

high conductivity of the plasma above a temperature of a few keV typically requires plasma currents which are larger than those allowed by MHD stability constraints. For non-tokamak devices such as mirrors and stellarators, supplementary heating must provide all the energy to reach ignition conditions.

The most successful auxiliary heating method to date has been injection of high energy neutral beams[6,7]. Unfortunately, this method has an uncertain future due to the technological complexity and expense of producing the high beam energies (>200 keV) that would be required for a reactor. At present, one of the most promising techniques for bringing tokamaks to ignition appears to be radio frequency (rf) heating. This method heats the plasma through the absorption, and subsequent thermalization, of electromagnetic wave energy which is generated by antennas near the plasma boundary. This is a versatile technique in that one can choose which class of particles the waves couple to, and in general the location in the plasma where the energy is deposited. The three most studied techniques have been Ion Cyclotron Resonance Heating (ICRH)[8,9], Electron Cyclotron Resonance Heating (ECRH)[10,11], and Lower Hybrid Heating (LHH)[12]. Each of these techniques has achieved some measure of success, with each having specific weaknesses and strengths. However, no single one of these has as yet proven itself as the method of choice for a tokamak

reactor. There is still plenty of room for, and interest in, new rf heating concepts.

This thesis will be concerned with one of the more promising of these new concepts, namely Shear Alfvén Resonance Heating (SARH). Although utilization of the shear Alfvén resonance for heating tokamaks was proposed more than ten years ago by Hasegawa and Chen[13] and Tataronis and Grossmann[14], it has only been in the last five years that experimental application of the technique to tokamaks has begun. There is currently a great deal of interest in this technique as promising new results appear. This is evidenced by the rapidly increasing number of both experimental and theoretical papers on SARH appearing in the literature and at plasma conferences during the past several years.

There are presently five experiments on SARH in tokamaks worldwide. The largest of these is on the TCA tokamak at Lausanne, Switzerland[15]. TCA is a medium sized tokamak built specifically to test SARH in a tokamak[16]. It has been operating since 1980 and has recently reported the first observation of ion and electron heating utilizing SARH in a tokamak[17]. Another experiment has been on the Pretext tokamak at the University of Texas, Austin[18]. They have concentrated on loading measurements with various antennas, and on CO_2 laser scattering experiments to observe wave phenomena. As of this writing, they have apparently observed the discrete global

Alfvén wave[19], but have yet to observe the shear resonance. Unfortunately, this experiment is being terminated. At the University of Wisconsin, Madison, we have concentrated on identifying the shear resonance directly through probe measurements[20], and are now involved in high power heating experiments[21]. Two other somewhat smaller experimental efforts are also underway on the Tortus tokamak at the University of Sidney, Australia[22] and in the RO-5 tokamak in the USSR[23]. Both have recently reported interesting results. Their experiments are only just beginning, however. Some earlier experiments were performed on a linear theta pinch[24] and in stellerator devices[25].

Just what are the features of SARH that have generated so much recent interest in this technique? Probably the single most appealing feature of SARH is its frequency range. A tokamak will probably need upwards of 100 MW of supplementary heating power to reach ignition. For the frequency range of SARH this is not a problem, involving essentially off-the-shelf technology. However, as the operating frequency regime for each technique rises, the technology to produce this power level becomes less available and more expensive. Table 1.1 puts SARH in context with the other three main rf heating methods.

A very appealing feature of SARH is that the energy is theoretically deposited on a magnetic flux surface, rather than

TABLE 1.1

	SARH	ICRH	LHH	ECRH
GENERATION				
frequency	1-2 MHz	50-100 MHz	1-5 GHz	50-200 GHz
sources	tubes	tubes	klystrons	gyrotrons
generation efficiency	90%	70%	60%	40%
attainable power per generator	10 MW	1-2 MW	1 MW	0.2 MW
TRANSMISSION				
method	coaxial line	coaxial line or ridged waveguide	waveguide	waveguide
power/line	10 MW	2 MW	1 MW	0.2 MW
COUPLING				
technique	loop antenna	loop antenna or cavity-backed aperture antenna	flush-mounted waveguide array with specified phases	flush-mounted waveguide array
mode-tracking?	no	maybe	no	no

in a cylindrical surface as for ICRH and ECRH. This feature could allow for the possibility of more uniform heating of the plasma, especially the plasma core. This feature could also provide a powerful method of profile modification through radially localized heating to adjust the local conductivity, current density, and temperature.

There is currently a great deal of interest in operating tokamaks in a steady state to eliminate the engineering problems associated with pulsed operation. Hasegawa[26], and Fisch and Karney[27] have suggested using Alfvén waves for current drive in a tokamak which could ultimately be as important as its heating function.

Unfortunately, there are also a few negative features associated with SARH. The most important of these is again more of a practical nature. Namely, the antenna requirements at lower frequencies seem to be more stringent. In principle, the lower frequencies would seem to require physically larger antennas. Since the mode that one is trying to drive in SARH is helical in nature, ideally one would then drive it with a helical antenna which wraps around the plasma current channel. This would be unfeasible for a reactor, since the antenna must be close to the edge of the plasma and shielding from the heat and neutron load would be a considerable problem. The solution appears to be to use several localized antennas somewhat similar to the antenna loops of ICRH. When properly located

and phased, coupling to the helical shear Alfvén mode would be possible. If efficient coupling can be attained with this technique then the antenna problem may turn out not to be any worse than that for ICRH. There are also other ideas for solving this problem, using different antenna designs, e.g. cavity resonators[28].

Other problems that may appear are enhanced radial transport induced by the rf fields and coupling to deleterious modes causing instabilities to occur. However, the recent heating results[17] from TCA have apparently not shown any degradation of confinement due to the rf and so these fears may turn out to be unfounded.

The experimental base for SARH in a tokamak is still in a very early stage of development with most of the theory, including that pertaining to the resonance itself, yet to be confirmed by experiment. This is quite similar to the state ICRH was in about 20 years ago when the basic concept had been established, but there existed little experimental data to confirm the theory. The shear Alfvén resonance has been directly observed in linear devices[29] and somewhat less directly in stellarators[30], but has not heretofore been observed in a tokamak.

The first most obvious question to ask about SARH in tokamaks from the outset, is whether the shear Alfvén resonance actually exists in a tokamak with the properties predicted by

MHD theory. If this most basic prediction of the theory were incorrect, then one could never hope to fully understand a heating experiment based on this theory. It thus seemed prudent to precede a high power heating experiment with careful identification of the resonance in a tokamak at lower power levels. With an identification firmly in hand, we could then confidently attack the heating experiment from a firm theoretical basis.

The resonance is most easily identified through its wave magnetic field inside the plasma, which is relatively straightforward to measure (for low temperature plasmas) and is a direct indicator of the resonance in the following sense. Since the resonance is an MHD resonance (i.e. predictable from MHD theory) we were guided in the design of the experiment primarily by MHD theory. According to MHD, three perturbation quantities are associated with the wave--the wave fluid velocity $\underline{\tilde{v}}$, magnetic field $\underline{\tilde{B}}$, and plasma pressure $\tilde{p}$. At the resonant location, where the drive frequency and mode structure of the external antenna provides a match to the local Alfvén velocity, $\underline{\tilde{v}}$ is predicted to be infinite, but this is not a readily measurable quantity in a plasma. $\underline{\tilde{B}}$ also becomes infinite and can be measured in Tokapole II with magnetic probes. The perturbed pressure of the wave is a somewhat indirect indicator of the resonance. If the equilibrium plasma pressure is zero (a good approximation for the low beta

Tokapole II plasma), MHD implies that $\tilde{p}$ is strictly zero everywhere. If the equilibrium pressure is nonzero, $\tilde{p}$ does blow up at the resonance, but much more weakly than $\underline{\tilde{B}}$. In fact, at the resonance $\tilde{p}/\tilde{B}$ goes to 0 even though $\tilde{p}$ and $\underline{\tilde{B}}$ both go to infinity. For typical measured values of $\tilde{B}$ in these experiments, $\tilde{p}/p < 10^{-4}$. Thus the plasma pressure is both indirect and difficult to measure. $\underline{\tilde{B}}$ is the observable of choice since it is both strongly divergent and measurable. This thesis will therefore concentrate almost exclusively on the magnetic field measurements of the resonance.

This thesis describes the initial experimental work performed for the Shear Alfvén Resonance Heating project at the University of Wisconsin. This is perceived as being a long-term research project with at least two follow-on theses. It is presently one of only two Alfvén heating programs in the United States, the other one being on the Pretext device at Texas. As of this writing, however, the experiment on Pretext appears to be in the final stages of being terminated.

In this thesis, we will describe measurements of the spatial and temporal properties of the resonance in a tokamak, and compare these results with MHD theory. In addition, the radial location of the resonance is compared with a two-dimensional calculation by Kieras and Tataronis[31,32] in which the ideal MHD equations are solved for the Tokapole II device, thereby including both toroidicity and noncircularity

of the plasma cross-section. We will show that, in all points, the measured resonance properties are consistent with those predicted by the theory. In doing this, we present what we believe to be a convincing case for the first direct observation of the shear Alfvén resonance in a tokamak.

In chapter 2 the basic theoretical model of the shear Alfvén wave in a non-uniform plasma is developed from MHD theory. Since kinetic effects are not critical to the results of this thesis, we give only cursory coverage to this topic. Finally, a brief summary of the analytical results obtained by Kieras and Tataronis for tokamaks and their numerical application to the Tokapole II device is presented.

Chapter 3 presents a description of Tokapole II and general machine hardware. The characteristics of typical plasma discharges are described along with the primary plasma diagnotics used.

A description of the rf apparatus used in this experiment is given in Chapter 4. This covers the launching structures, rf sources and magnetic probes. The two most difficult problems that had to be dealt with on a constant basis in this experiment were rf pickup on the diagnotics, especially on magnetic probes, and the struggle to construct probes that not only survived the discharge but that did not perturb the discharge significantly. This is also discussed in Chapter 4 which describes how these problems were eventually solved.

Chapter 5 presents the experimental data supporting the identification of the shear Alfvén resonance. The data are compared with the theoretical predictions from MHD, and the radial locations are shown to be in good agreement with the numerical calculations (of Kieras and Tataronis).

Chapter 6 summarizes the experimental results and makes suggestions for future experiments.

In this thesis, references will be made from time to time to PLP reports. These are internal papers of the University of Wisconsin Plasma Physics Group. Copies are available on request from:

Plasma Physics Department
University of Wisconsin
1150 University Ave.
Madison, WI 53706

REFERENCES - CHAPTER 1

1. E.M. Barston, Ann. Phys. 29, 282 (1964).

2. C. Uberoi, Phys. Fluids 15, 1673 (1972).

3. L.A. Artsimovich, Nucl. Fusion 2, 215 (1972).

4. H.P. Furth, Nucl. Fusion 15, 487 (1975).

5. J. Sheffield, Proc. IEEE 69, 885 (1981).

6. M.M. Menon, Proc. IEEE 69, 1012 (1981).

7. W. Stodiek, et al., IAEA-8, CN-38/A-1 (1980).

8. T.H. Stix, The Theory of Plasma Waves (McGraw-Hill, New York, 1962).

9. P.L. Colestock, C. Barnes, M. Bitter, D. Boyd, N. Bretz, et al., in Proceedings of the Fifth Topical Conference on Radio Frequency Plasma Heating (Madison, 1983).

10. R.M. Gilgenbach, et al., Phys. Rev. Lett. 44, 647 (1980).

11. C.P. Moeller, in Proceedings of the Fifth Topical Conference on Radio Frequency Plasma Heating (Madison, 1983).

12. T. Imai, T. Yamamoto, N. Suzuki, K. Uehara, et al., ibid.

13. A. Hasegawa and L. Chen, Phys. Rev. Lett. 32, 454 (1974); Phys. Fluids 17, 1399 (1974).

14. W. Grossmann and J. Tataronis, Z. Physik 261, 203 and 217 (1973).

15. A. DeChambrier, et al., Plasma Physics 24, 893 (1982); R. Keller, et al., in 4th Topical Conf. on RF Heating in Plasmas, (Austin, 1981).

16. A.D. Chettham, A. Heym, et al., CRPP Internal Report LRP 162/80, Lausanne (1980).

17. R. Behn, A. de Chambrier, et al., CRPP Internal Report LRP 232/83, Lausanne (1983).

18. D.W. Ross, et al., in 4th Topical Conf. on RF Heating in Plasmas, (Austin, 1981).

19. T.E. Evans, et al.; M.E. Oakes, et al.; and R.D. Bengtson, et al., Bull. Am. Phys. Soc. 28, 1085 (1983); R.D. Bengtson, et al., in 5th Topical Conf. on RF Heating in Plasmas, (Madison, 1983).

20. F.D. Witherspoon, et al., in 4th Topical Conf. on RF Heating in Plasmas, (Austin, 1981); S.C. Prager, et al., in 5th Topical Conf. on RF Heating in Plasmas, (Madison, 1983).

21. D. Kortbawi, F.D. Witherspoon, J.C. Sprott, and S.C. Prager, Bull. Am. Phys. Soc. 28, 1086 (1983).

22. R.C. Cross, et al., in Proc. 3rd Joint Varenna-Grenoble Int. Symp. Vol. I, 183 EUR7979EN (1982).

23. R.A. Demirkhanov, et al., in Proc. 9th Int. Conf. on Plasma Physics and Contr. Nucl. Fusion, (Baltimore, 1982).

24. R. Keller and A. Pochelon, Nucl. Fusion 18, 1051 (1978).

25. S.N. Golovato and J.L. Shohet, Phys. Fluids 21, 1421 (1978); K. Uo, et al., in Proc. 6th Int. Conf. on Plasma Phys. and Contr. Nucl. Fusion, IAEA-CN-37-L-1 (Berchtesgaden, 1976).

26. A. Hasegawa, Nucl. Fusion 20, 1158 (1980).

27. N. Fisch and C. Karney, Phys. Fluids 24, 27 (1981).

28. J.H. Mullen, Bull. Am. Phys. Soc. 28, 1043 (1983), F.P. Blau, S.C. Chiu, P.B. Parks, and J.M. Rawls, ibid., 1042.

29. A. Tsushima, Y. Amagishi, and M. Inutake, Phys. Letters 88A, 457 (1981).

30. S.N. Golovato and J.L. Shohet, Phys. Fluids 21, 1421 (1978).

31. C.E. Kieras, Ph.D. Thesis, University of Wisconsin (1982).

32. C.E. Kieras and J.A. Tataronis, J. Plasma Phys. 28, 395 (1982).

CHAPTER 2

THEORY

The existence of shear Alfvén waves in uniform plasmas has been well known for many years[1,2]. In a uniform plasma the Alfvén speed is constant, and the ideal MHD equations lead immediately to the dispersion relation for the propagation of small amplitude waves

$$\omega^2 = k_\parallel^2 v_A^2 = k_\parallel^2 B^2/\mu_o\rho$$

where $k_\parallel$ is the wave propagation vector and v_A is the Alfvén speed.

In nonuniform plasmas, such as those encountered in the laboratory, the Alfvén speed is no longer constant but is a function of position in the direction of the non-uniformity. In general there are non-uniformities in both density and magnetic field. Instead of a dispersion relation, the shear Alfvén wave now satisfies a resonance condition, where wave quantities $\to \infty$ and energy is absorbed at the location within the plasma where the frequency and parallel wave vector satisfy the local Alfvén speed, i.e.

$$\omega_o = k_\parallel v_A(x_o)$$

where x_o is the location where this condition is satisfied for the given ω_o and $k_\parallel$ which are usually specified by external oscillators and wave coupling structures.

The basic theoretical model for this resonance condition and its applicability to plasma heating was first suggested by Tataronis and Grossmann[3] and Hasegawa and Chen[4]. The first part of this chapter will follow Hasegawa and Chen in the derivation of the resonance condition. In the following sections we will follow Kappraff and Tataronis[5] to estimate the radial widths and risetimes of the resonances due to ohmic dissipation. We will then briefly discuss the "kinetic Alfvén wave" and some of its implications to heating. Finally, we will discuss toroidal effects in the MHD model following the work of Kieras and Tataronis[6,7]

a. Basic model

Following Hasegawa and Chen, we assume a one dimensional ideal MHD slab model with the non-uniformity in the x direction, i.e. the mass density ρ, pressure p, and equilibrium magnetic field $\underline{B}$ varying only as functions of x. The magnetic field is straight but has shear, i.e.

$$\underline{B}(x) = B_z(x)\hat{z} + B_y(x)\hat{y} \qquad (1)$$

Note that to extend these results to a toroidal plasma, x, y,

and z would correspond to the radial, poloidal, and toroidal directions respectively.

By linearizing the ideal MHD equations for small wave amplitudes, we are immediately led to the differential equation for the fluid displacement vector $\underline{\xi}$

$$\mu_o \rho \ddot{\underline{\xi}} - (\underline{B}\cdot\nabla)^2 \underline{\xi} = -\mu_o \nabla \tilde{p} - \underline{B}(\underline{B}\cdot\nabla)(\nabla\cdot\underline{\xi}) \qquad (2)$$

where $\tilde{p}=p+\underline{b}\cdot\underline{B}/\mu_o$ is the total pressure to 1st order, and $\underline{b}$ is the 1st order perturbation in the magnetic field. $\underline{b}$ and $\underline{\xi}$ are related through Maxwell's equations

$$\underline{b} = \nabla\times(\underline{\xi}\times\underline{B})$$

or

$$\underline{b} = (\underline{B}\cdot\nabla)\underline{\xi} - \underline{B}(\nabla\cdot\underline{\xi}) - (\underline{\xi}\cdot\nabla)\underline{B} \qquad (3)$$

To close the MHD equations we assume an adiabatic equation of state (not linearized yet)

$$\frac{d}{dt}(p\rho^{-\gamma}) = 0$$

Combining this with the continuity equation

$$\frac{\partial p}{\partial t} + \nabla\cdot(\rho\underline{v}) = 0$$

and linearizing yields the perturbed plasma pressure in terms of $\underline{\xi}$

$$\tilde{p} = -\xi_x \frac{dp}{dx} - \gamma p(\nabla\cdot\underline{\xi}) \qquad (4)$$

Fourier analyzing along the symmetry directions, y and z, but not along the non-uniformity direction, yields perturbations of the form

$$\underline{\xi} = \underline{\xi}(x)\exp[i(k_z z + k_y y - \omega t)] .$$

Let us define a more convenient set of local orthogonal rectangular coordinates:

$$\hat{e}_x = \hat{x}, \quad \hat{e}_\parallel = \underline{B}/B, \quad \hat{e}_\perp = \hat{e}_\parallel\times\hat{e}_x .$$

In this coordinate system, Eq. (2) becomes for each component

$$\varepsilon\xi_\parallel = ik_\parallel\mu_o\tilde{p} + iB^2k_\parallel(ik_\parallel\xi_\parallel + ik_\perp\xi_\perp + \frac{d\xi_x}{dx}) \qquad (5)$$

$$\varepsilon\xi_\perp = ik_\perp\mu_o\tilde{p} \qquad (6)$$

$$\varepsilon\xi_x = \mu_o\frac{d\tilde{p}}{dx} \qquad (7)$$

In these expressions, $\varepsilon(x) = \omega^2\mu_o\rho - k_\parallel^2B^2$, $k_\parallel(x)B(x) = k_zB_z +$

$k_y B_y$, and $k_\perp(x)B(x) = k_y B_z - k_z B_y$. By using Eqs. (3) and (4), $\xi_\perp(x)$ can be expressed in terms of $\xi_x(x)$ as

$$\xi_\perp(x) = \frac{i\alpha k_\perp B^2}{\alpha k_\perp^2 B^2 - \epsilon}\frac{d\xi_x}{dx} \qquad (8)$$

where

$$\alpha(x) = 1 + \gamma\beta\omega^2/(\omega^2 - \gamma\beta k_\parallel^2 v_A^2)$$

and

$$\beta(x) = \frac{p}{B^2/\mu_o}$$

For plasmas with low β (as for tokamaks like Tokapole II), $\gamma\beta<<1$ which implies $\omega_o^2 >> \gamma\beta k_\parallel^2 v_A^2$, and we thus have $\alpha(x) = 1+\gamma\beta \sim O(1)$. Substitution of Eqs. (6) and (8) then leads to the wave equation for ξ_x

$$\frac{d}{dx}\left(\frac{\epsilon\alpha B^2}{\alpha k_\perp^2 B^2 - \epsilon}\frac{d\xi_x}{dx}\right) - \epsilon\xi_x = 0 \qquad (9)$$

Note that if the non-uniformity is removed, $\frac{d}{dx} \to 0$, and (9) reduces to

$$\epsilon\xi_x = 0$$

or

$$(\omega^2\mu_o\rho - k_\parallel^2 B^2)\xi_x = 0 \qquad (10)$$

thus recovering the shear Alfvén wave in a uniform plasma. The compressional wave is recovered by letting $\frac{d}{dx} \to ik_x$, which immediately yields the dispersion relation for the compressional Alfvén wave,

$$\omega^2 = k^2 v_A^2 .$$

Eq. (9) has a singular solution when the leading coefficient is zero. This occurs at the location $x=x_o$ where $\epsilon=0$, i.e. when $\omega = k_\parallel v_A(x)$. Near $x=x_o$

$$\epsilon(x) = \left(\frac{d\epsilon_r}{dx}\right)_{x_o}(x-x_o)$$

where ϵ_r is the real component of ϵ. (An artificial dissipation can be included in the analysis by including a small imaginary component, ϵ_i in ϵ.) Using this Taylor expansion of $\epsilon(x)$ to evaluate Eq. (9) near $x=x_o$ yields

$$\frac{d^2\xi_x}{dx^2} + \frac{1}{x-x_o}\frac{d\xi_x}{dx} - k_\perp^2\xi_x = 0 \qquad (11)$$

The approximate solution for ξ displays a logarithmic singularity near $x=x_o$.

$$\xi_x = C\ \ln(x-x_o). \qquad (12)$$

We are also interested in determining the behavior of the

other perturbation wave fields near the resonance. Specifically, we are interested in determining b_x, $b_\perp$, $b_\parallel$ near the resonance. We can then compare experimental measurements with these predictions.

In the low β limit $\hat{p} = \underline{b}\cdot\underline{B}/\mu_o$. Thus Eq. (7) can be rewritten as

$$\varepsilon\xi_x = \mu_o \frac{d}{dx}(\underline{b}\cdot\underline{B}/\mu_o)$$

$$= \frac{d}{dx}(b_\parallel B) = Bb_\parallel' \ .$$

Near the resonance, $\xi_x \sim \ln(x-x_o)$ which diverges, but $\varepsilon \sim (x-x_o)$. Since $(x-x_o)\ln(x-x_o) \to 0$ as $x \to x_o$ this implies that $b_\parallel' = 0$, and thus that $b_\parallel$ = constant.

Next, Eq. (6) can be written as

$$\varepsilon\xi_\perp = ik_\perp b_\parallel B$$

Thus

$$\xi_\perp(\omega) = ik_\perp b_\parallel B/\varepsilon \sim \frac{1}{x-x_o(\omega)} \ .$$

Taking the x-component of Eq. (3) yields

$$b_x = ik_\parallel B\xi_x \sim \ln(x-x_o)$$

And finally taking the $\perp$-component of Eq. (3) yields

$$b_\perp = iBk_\parallel\xi_\perp \sim \frac{1}{x-x_o(\omega)}$$

Even though we have now determined all the fields, for completeness we would also like to determine the behavior of $\xi_\parallel$ at the resonance. To do this look at the force balance equation

$$\rho\frac{d\underline{v}}{dt} = \underline{J}\times\underline{B} - \nabla p$$

Taking the parallel component of this equation we obtain

$$\rho\frac{dv_\parallel}{dt} = 0$$

or

$$\omega^2\rho\xi_\parallel = 0$$

since the terms on the right hand side are all $\perp$ to the equilibrium field.

To summarize the wave field behavior at the resonance, we have

$$\xi_{\parallel} = 0$$

$$\xi_{\perp} \sim \frac{1}{x-x_o(\omega)}$$

$$\xi_x \sim \ln(x-x_o(\omega))$$

$$b_{\parallel} \sim \text{constant}$$

$$b_{\perp} \sim \frac{1}{x-x_o(\omega)}$$

$$b_x \sim \ln(x-x_o(\omega))$$

All the quantities we have been dealing with so far, i.e. $\underline{\xi}$ and $\underline{b}$ are the transform variables in frequency space. To determine the time behavior of these quantities, we must perform an inverse Laplace transform. This has been done by Tataronis[9], assuming a forcing function to represent an external coupler at a driving frequency of ω_o. This yields the following time behavior for the fields:

$$b_{\parallel}(t) \sim \sin \omega_o t$$

$$b_{\perp}(t) \sim t \sin\omega_o t$$

$$b_x(t) \sim \ln t \sin\omega_o t \ .$$

We thus see that the wave magnetic field parallel to the equilibrium field simply oscillates and does not grow in amplitude. Both the radial component and the perpendicular component (which lies in a flux surface for a tokamak) are divergent in time with the perpendicular component being more strongly divergent than the radial component. It is the perpendicular component of the wave field that is studied experimentally in this thesis.

In the same paper, Tataronis calculates the energy absorption rate for ideal MHD by taking the dot product of $\underline{v}$ with the linearized momentum conservation equation and then integrating over the plasma volume, forming thus an energy equation for ideal MHD. The resulting expression is

$$W = \frac{2\pi L_y}{k}\int_0^a dx \left\{ \frac{1}{2}\rho(x)\underline{v}^2(x,t) + \frac{1}{2\mu_o}k^2B^2(x)\underline{\xi}^2(x,t) \right\}. \qquad (13)$$

where L_y is the plasma extent in the y direction, a corresponds to the radius of the plasma (the x-direction) and the integral along the z-direction extends for one wavelength in the z-direction, and $\underline{v} = \frac{d\underline{\xi}}{dt}$. The first term represents the wave

kinetic energy while the second term represents a wave potential energy.

Since the perpendicular components of the wave fields are non-square integrable, the wave energy grows without bound, accumulating in an infinitesimally narrow region about the singular surface. The fields away from the resonant surface simply oscillate at constant amplitude while those at the resonant surface grow in time. For a real plasma, dissipative processes should be considered. However, before discussing that, let us digress briefly to make a connection with experiment.

The design of a coupling structure which can drive these resonant modes can be qualitatively understood from the screw-pinch model. The resonance occurs when $\varepsilon = 0$, i.e. when

$$\omega^2(r) = (\underline{k}\cdot\underline{v}_A)^2$$

or

$$\omega^2(r) = (k_z B_z + k_\theta B_\theta)^2/\mu_o\rho$$

where again z and θ are the axial and azimuthal directions, respectively and r is the minor radius. To make the connection to a tokamak, this expression can be rewritten as

$$\omega^2(r) = (n + \frac{m}{q})^2 B_z^2/\mu_o\rho R^2 \qquad (14)$$

where q is the safety factor, rB_z/RB_θ, R is the major radius and n and m are the toroidal and poloidal mode numbers respectively. The approximations $k_z = k_\zeta = n/R$ and $k_\theta = m/r$ have been made. In general, the coupling structure should have the same toroidal and poloidal mode structure as the resonant mode, covering as large a fraction of the plasma surface area as is physically possible. Ideally, sheet currents which completely enclose the plasma are the best, and many theoretical calculations assume just such a current distribution[9,10,11]. In reality, such current distributions can be approximated by line currents which wind around the plasma cross-section in a helical fashion (see Figure 4-1). By choosing toroidal and poloidal mode numbers of opposite sign, it is possible to obtain resonant frequencies that are quite low. This is one of the more interesting aspects of SARH from a practical point of view, since it allows for the possibility of heating at the relatively low frequency range of ~ 1 MHz, for which a mature rf technology exists.

b. Dissipation

In the ideal MHD model, as time $t \to \infty$ the wave fields grow indefinitely and the resonance width, Δ, approaches zero. In a real plasma, dissipation of the wave fields by the plasma will

keep $\underline{b}$ and Δ finite. A resistive MHD boundary layer calculation has been performed by Kappraff and Tataronis[5] in which resistivity η was included in a thin layer about the resonant surface and assuming ideal MHD outside this thin layer, with the solutions in the two regions matched at the boundary.

Their analysis revealed two time scales which characterize the energy absorption process. Up to some critical time, τ_{rise}, which scales as $\eta^{-1/3}$, the incoming energy accumulates about the resonant surface just as in the ideal MHD case. This scaling is a result of matching solutions at the boundaries between the resistive layer and the surrounding ideal regions. For times greater than this, the growing resonant wave fields in the resistive layer have saturated in amplitude and the incoming energy is transferred to heat through ohmic heating of the electrons. The idea is illustrated in Figure 2-1, which comes from their paper.

The expression they derived for the time to saturate is

$$\tau_{rise} \approx \left(\frac{24\mu_o}{\omega_o^2 \eta}\right)^{1/3} \left(2\frac{B'}{B} - \frac{\rho'}{\rho}\right)^{-2/3} \qquad (15)$$

where the prime indicates derivatives with respect to the non-uniformity direction x, and all quantities are evaluated at the singular surface $x=x_o$.

To lowest order in the resistivity, they found the rate of

Fig 2-1. Growth of the wave fields in the ideal and resistive MHD cases.

WITH ABSORPTION

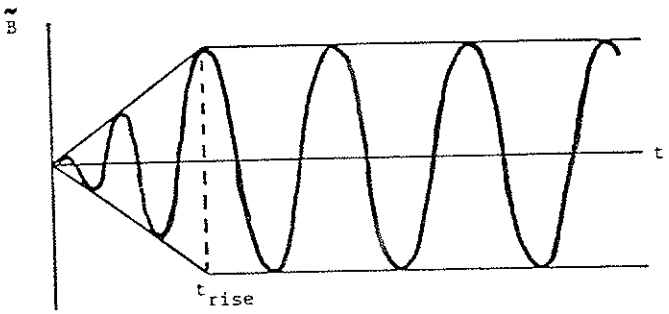

IDEAL MHD

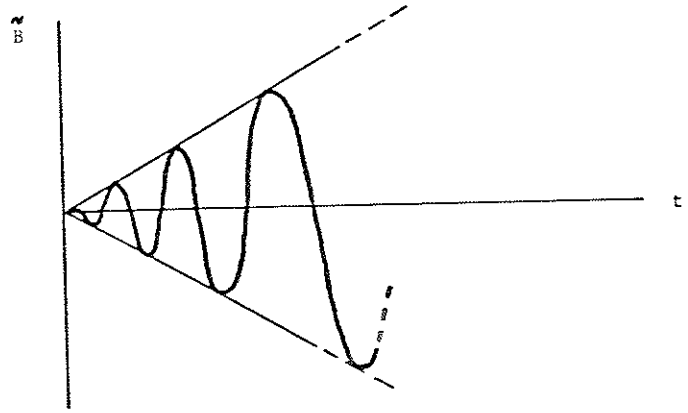

absorption to be equal to that of the ideal MHD case. An estimate of the resistive width can then be obtained by formally setting the heating rate due to ohmic heating (integrated around some small layer of width Δx) to the ideal MHD heating rate as calculated in Tataronis[8]. In other words,

$$\int_{plasma} \eta j^2 dx = \left(\frac{dW}{dt}\right)_{ideal\ MHD}$$

Assuming a constant η in the resistive layer and $\eta=0$ everywhere else, the following estimate for the resistive width was obtained

$$\Delta x \approx .8\pi \left(\frac{\eta}{\mu_o \omega_o}\right)^{1/3} \left(2\frac{B'}{B} - \frac{\rho'}{\rho}\right)^{-1/3} \qquad (16)$$

We will use these expressions in Chapter 5 to estimate the predicted radial width and risetime of the observed resonances.

c. Kinetic effects

In order to obtain a more realistic picture of the resonance in a collisionless plasma, such as would be encountered in a reactor, effects due to electron inertia, finite ion gyroradius, and dissipative processes such as ion viscosity, electron collisions, Landau damping, and nonlinear

processes must be included. This has been done by Hasegawa and Chen[12] and Ross[10].

When the perpendicular wavelength $2\pi/k_\perp$ becomes comparable in magnitude to the ion gyroradius, ρ_i, ions can no longer be considered tied to the field lines, whereas the lighter electrons are still tied. Wave motion thus induces a charge separation and a coupling to the electrostatic mode. Including these effects leads to the kinetic Alfvén wave, whose dispersion relation is given by

$$\omega^2 = k_z^2 v_A^2 [1 + k_\perp^2 \rho_i^2 (\tfrac{3}{4} + \tfrac{T_e}{T_i})] .$$

Due to the small $k_\perp$ this kinetic Alfvén wave can propagate across the magnetic field and can be dissipated by both electron and ion Landau damping on the $E_\parallel$ associated with the wave. (There is no $E_\parallel$ in the ideal MHD case since no charge separation arises.) This dispersion relation holds for $v_{T_e} > v_A$. If the opposite is true, then the dispersion relation must be modified to

$$\omega^2 = k_z^2 v_A^2 (1 + k_\perp^2 \rho_i^2)\left(1 + \frac{k_\perp^2 c^2}{\omega_{pe}^2}\right)^{-1}$$

The physical importance of this is that for $\beta < m_e/m_i$ (or equivalently $v_{T_e} < v_A$), where $\beta = p/(B^2/\mu_o)$ is the plasma beta, the kinetic wave will propagate to the lower density side of

the mode conversion surface. In a tokamak this would be towards the plasma edge, thus causing edge heating, which is not desired. For $\beta > m_e/m_i$, the wave propagates to the higher density side and can thus heat the plasma core. If the damping rate of the wave as it spirals in towards the core is such that it completely damps away by the time it reaches the center, then this process could provide a very uniform method of heating the plasma core. If the damping rate is very fast (relative to plasma scale lengths) then the wave energy will be deposited closer to the mode conversion surface, in which case it could provide not only heating, but also provide a means of modifying plasma profiles through local adjustments of the temperature and conductivity.

The singular surface of ideal MHD is removed by the non-ideal effects. However, the qualitative processes of the wave are similar, with only the addition of a large k_x (wave vector in the radial direction). The singular surface is replaced by a mode conversion layer where the incoming wave, from the external coupler, is converted into the kinetic Alfvén wave which then spirals into the plasma core. Hasegawa and Chen have shown that as long as the wave is completely damped before reaching the center of the plasma (no wave reflection), then the absorption is the same as that calculated for the ideal MHD case.[12]

Hasegawa and Chen also calculate the wave fields assuming

some given source term, which represents the external coupler. They find that the poloidal wave field at the mode conversion layer is enhanced over the corresponding vacuum wave field from the coupler. The enhancement factor is given by the expression

$$|B_{pol}| \sim (\kappa\rho_i)^{-2/3}[1 + (T_e/T_i)k_x^2\rho_i^2]\ |B_{pol\ vac}| \qquad (17)$$

where $B_{pol\ vac}$ is the vacuum wave field strength produced by the external antenna. For a reactor, where $\kappa \sim r^{-1} \sim 10^{-3}\rho_i^{-1}$, this enhancement can be as large as 100. For Tokapole II it is somewhat less as will be seen in Chapter 5.

As a final point to consider in this section, we can also make some rough estimates of the width of the resonance due to ion viscosity and electron Landau damping. Hasegawa and Chen[12] give expressions for the heating rates due to ohmic heating, ion viscosity, and electron Landau damping. Arguing heuristically that the width should scale as the heating rate to the 1/3 power, as Tataronis found for the resistive MHD case (since heating rate $\sim \eta$), we calculate the ratios of heating rates of ion viscosity and electron Landau damping to the ohmic heating rate. For ion viscosity we get

$$\frac{(dW/dt)_{ion\ viscous}}{(dW/dt)_{ohmic}} \sim \left(\frac{m_i}{m_e}\right)^{1/2} \left(\frac{T_i}{T_e}\right)^{3/2} \frac{1}{\beta_i} \qquad (18)$$

where $\beta_i = 2v_{T_i}^2/v_A^2$.

For electron Landau damping (ELD) we get

$$\frac{(dW/dt)_{ELD}}{(dW/dt)_{ohmic}} \sim \frac{\omega\nu_{ei}}{\delta_e k_z^2 v_{T_e}^2} \qquad (19)$$

We will make use of these expressions in Chapter 5.

d. Toroidal effects

It is not clear a priori that the results of the screw-pinch model are immediately applicable to the case of a tokamak for the following reason. The screw-pinch model has two degrees of symmetry, the axial and the azimuthal directions. All quantities are functions only of the radius r. This means, in particular, that the resonance condition given by Eq. (11) is satisfied, for ω_o, at a given radius $r = r_o(\omega_o)$. A resonant surface has constant radius and is thus also a magnetic surface. Each surface has a different resonant frequency, given by Eq. (11), thus giving rise to a continuous spectrum of frequencies. This simple resonance condition breaks down in a tokamak because surfaces of constant $k_\parallel v_A$ do not coincide with a magnetic surface due to the 1/R dependence of the toroidal magnetic field. Estimates for the shear Alfvén continuum frequencies in a tokamak based on the screw-pinch approximation may not, therefore, be particularly accurate.

Pao[13] and Goedbloed[14] were the first to treat the toroidal problem. They showed that by expressing the MHD equations in

the natural orthogonal flux coordinates of a toroidal system, that the continuum in an axisymmetric tokamak is determined by the eigenvalues of a set of coupled first order ordinary differential equations on each flux surface. It turns out that even though v_A is not constant on a flux surface, the eigenvalues are discrete on a given flux surface and cover a continuous range as the flux surface is varied from the magnetic axis out to the plasma edge. The radial eigenfunction can be shown to be singular on the resonant surface ψ_o, where $\omega_o^2 = \omega_A^2(\psi_o)$. This problem has also been treated by Tataronis, Talmadge and Shohet[15], Tataronis and Salat[16], Hameiri[17], and Hameiri and Hammer[18] for more general toroidal equilibria (for instance stellerators). None of these studies derived analytical expressions for the continua in a toroidal equilibrium.

Kieras[6,7] has taken this one step further by deriving analytic expressions for the shear Alfvén continuum for a large aspect ratio tokamak by solving the set of coupled differential equations on each flux surface. Toroidicity is included as a perturbation in the calculation utilizing an expansion in terms of the inverse aspect ratio $\varepsilon=a/R_o$, where a is the minor radius and R_o is the major radius of the plasma. The set of equations is then solved numerically. Specification of the equilibrium is provided by a numerical code[19] which solves the Grad-Shafranov equation in the poloidal divertor configuration

of Tokapole II, thereby including effects due to non-circularity of the plasma cross-section.

Kieras found that, to lowest order in this expansion, the continuum is given approximately by the continuum of the corresponding screw-pinch model. However, first order corrections due to the toroidicity cause a coupling between particular poloidal modes on rational q surfaces. Because of this coupling, gaps can form in the spectrum in which there are no continuum modes. (Chance and Cheng[20] have recently indicated the possibility of low toroidal number discrete modes occurring in the gap.)

This mode coupling can be explained by the following picture. In the simple screw-pinch model, it is possible for degeneracies to occur in the solution of the spectrum. This happens because on a given magnetic surface two different modes can have the same parallel wave number $k_\parallel = (m - nq)/r$ and hence the same resonant frequency. This is illustrated in Figure 2-2 where the degeneracy occurs at the q=3/2 surface.

The degeneracy in the cylindrical case is removed by the toroidal perturbation as illustrated in Figure 2-3. Here, the dashed curve represents the radial dependence of the resonant frequency for a cylinder showing the degeneracy of the (m,n) = (2,2) and (3,2) modes. The solid curves represent the solution with toroidicity included. The degeneracy is removed by a coupling or mixing of the two modes forming a gap in the

Fig. 2-2. Degeneracy in the cylindrical model occurs when two modes have the same $k_{\parallel}$. For the case shown, degeneracy occurs at the q = 3/2 surface.

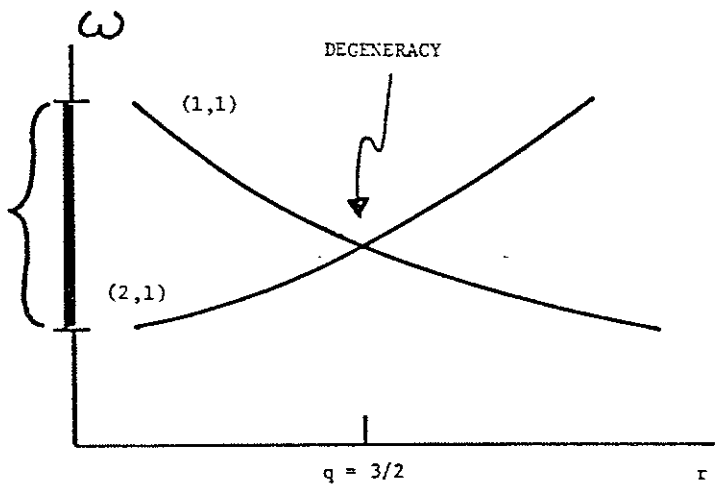

$$k_{\parallel} \sim m - nq$$

Thus

$$k_{\parallel}|_{(1,1)} \sim 1 - \frac{3}{2} = -\frac{1}{2} \qquad \text{at} \quad q = \frac{3}{2}$$

$$k_{\parallel}|_{(2,1)} \sim 2 - \frac{3}{2} = \frac{1}{2} \qquad \text{at} \quad q = \frac{3}{2}$$

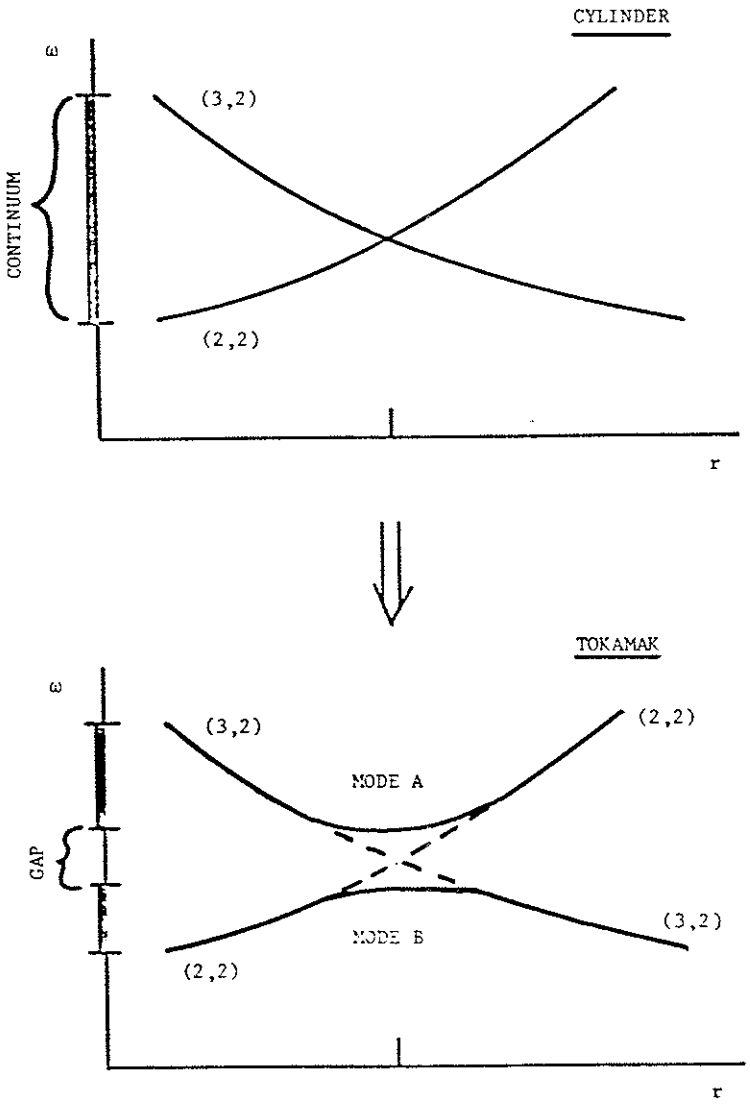

Fig. 2-3. Removal of the degeneracy in a cylinder by toroidal effects causing mode coupling between poloidal modes with same toroidal mode number.

frequency spectrum in which no resonance exists. The reason for the gap is revealed through the poloidal structure of the two modes, labelled A and B in the figure. At radii far from the mode coupling surface (where the degeneracy had existed) mode A is nearly a pure m=3 mode on the inside or a pure m=2 mode on the outside (of the torus). The mode labelled B is just the opposite. Right at the mode-coupling surface both modes A and B are a mixture of m=2 and m=3 modes as shown in Figure 2-4. In fact, modes A and B have identical structures there except for being shifted 180° in poloidal angle. Mode A peaks in the high field, high v_A, inner region of the torus and thus has a higher resonant frequency than the mode B which peaks in the low field, low v_A, outer region of the torus.

Kieras points out that this gap which forms due to coupling of degenerate poloidal modes is analogous to the gap which forms in the energy spectrum of electrons in a periodic crystal lattice. For that case, gaps form because of wave localization in either the high or low potentials in the regions near or in between the ion lattice sites. Similarly, gaps form in the Alfvén spectrum because of mode coupling between poloidal modes which tends to localize the eigenfunctions in regions of high and low Alfvén velocity corresponding to the high or low field regions of the toroid.

The importance of this gap formation is that it predicts that at certain oscillator frequencies and antenna mode

Fig. 2-4: Poloidal mode structure of coupled modes at mode coupling surface shows a mixing of the poloidal modes.

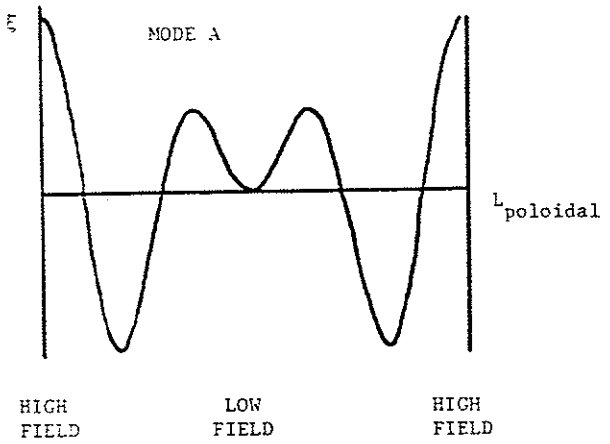

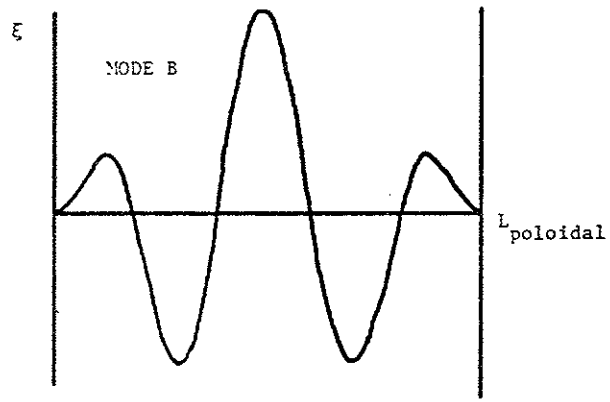

structures (helicities) it may not be possible to heat the plasma.

For further details concerning the analytical and numerical work of Kieras, the interested reader is directed to references 6 and 7.

REFERENCES - CHAPTER 2

1. A. Hasegawa and C. Uberoi, The Alfven Wave, Technical Information Center, USDOE (1982).

2. T.H. Stix, The Theory of Plasma Waves (McGraw-Hill, New York, 1962), Chapters 1 and 2.

3. W. Grossmann and J. Tataronis, Z. Physik 261, 203 and 217 (1973).

4. A. Hasegawa and L. Chen, Phys. Rev. Lett. 32, 454 (1974); Phys. Fluids 17, 1399 (1974).

5. J.M. Kappraff and J.A. Tataronis, J. Plasma Phy. 18, 209 (1977).

6. C.E. Kieras, Ph.D. Thesis, University of Wisconsin (1982).

7. C.E. Kieras and J.A. Tataronis, J. Plasma Phys. 28, 395 (1982).

8. J.A. Tataronis, J. Plasma Phys. 13, 87 (1975).

9. J.A. Tataronis and W. Grossmann, Nucl. Fusion 16, 667 (1976).

10. D.W. Ross, G.L. Chen, and S.M. Mahajan, Phys. Fluids 25, 652 (1982).

11. J.A. Tataronis and W. Grossmann, Courant Institute of Mathematical Sciences, NYU, Report MF-84, COO-3077-102 (1977).

12. A. Hasegawa and L. Chen, Phys. Fluids 19, 1924 (1976).

13. Y.P. Pao, Nucl. Fusion 15, 631 (1975).

14. J.P. Goedbloed, Phys. Fluids 18, 1258 (1975).

15. J.A. Tataronis, J.N. Talmadge, and J.L. Shohet, Proc. 3rd Topical Conf. on RF Plasma Heating, (Pasadena, 1978), also Comments Plasma Phys. Controlled Fusion 7, 29 (1982).

16. J.A. Tataronis and A. Salat, Proc. 2nd Joint Grenoble-Varenna Int. Symp. on Heating in Toroidal Plasmas, (Como, Italy, 1980).

17. E. Hameiri, Phys. Fluids 24, 562 (1981).

18. E. Hameiri and J.H. Hammer, Phys. Fluids 22, 1700 (1979).

19. M.W. Phillips, University of Wisconsin PLP 765 (1978).

20. M.S. Chance and C.Z. Cheng, Sherwood Theory Conference, paper 1P10 (1984).

CHAPTER 3

TOKAPOLE II

3.A. Machine description

The experiments described in this thesis were performed on the Tokapole II device at the University of Wisconsin[1]. Tokapole II (Figure 3-1) is a small tokamak which operates in a four-node poloidal divertor configuration which is formed by four internal field shaping rings. More complete descriptions of the device can be found elsewhere[2,3].

The vacuum vessel is an aluminum torus with a major radius of 50 cm and a square cross-section 44 cm on a side (Figure 3-2). Since field soak-in time for the 3 cm thick aluminum wall is about 15 msec, insulated gaps in both the toroidal and poloidal directions are provided in order to allow the magnetic fields to enter the machine. Vacuum is maintained by a 1500 l/sec turbomolecular-pump, which typically yields base pressures of low 10^{-7} Torr when the system is clean and relatively leak-free. Both Taylor[4] and glow discharge[5] cleaning have been used to condition the walls overnight and after bringing the system up to atmospheric pressure.

The field shaping rings are located at the four corners of the vacuum vessel (Figure 3-2). Each ring is made of a high conductivity chromium-copper alloy with a minor cross-sectional

Fig. 3-1. Tokapole II.

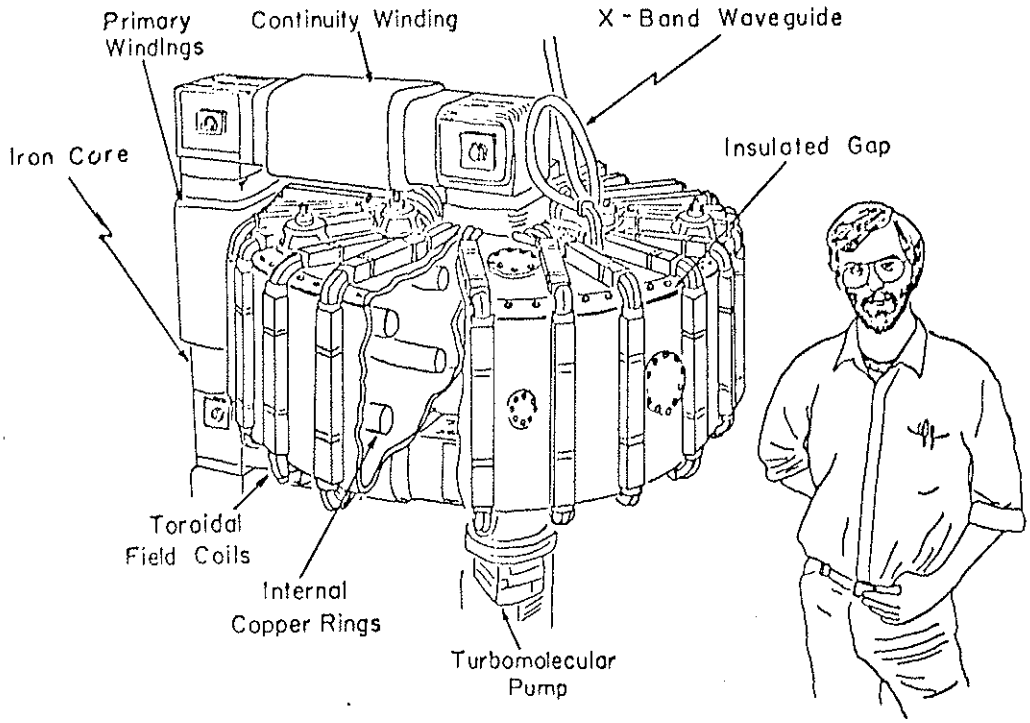

TOKAPOLE II

Fig. 3-2: Cross section of vacuum vessel showing internal rings.

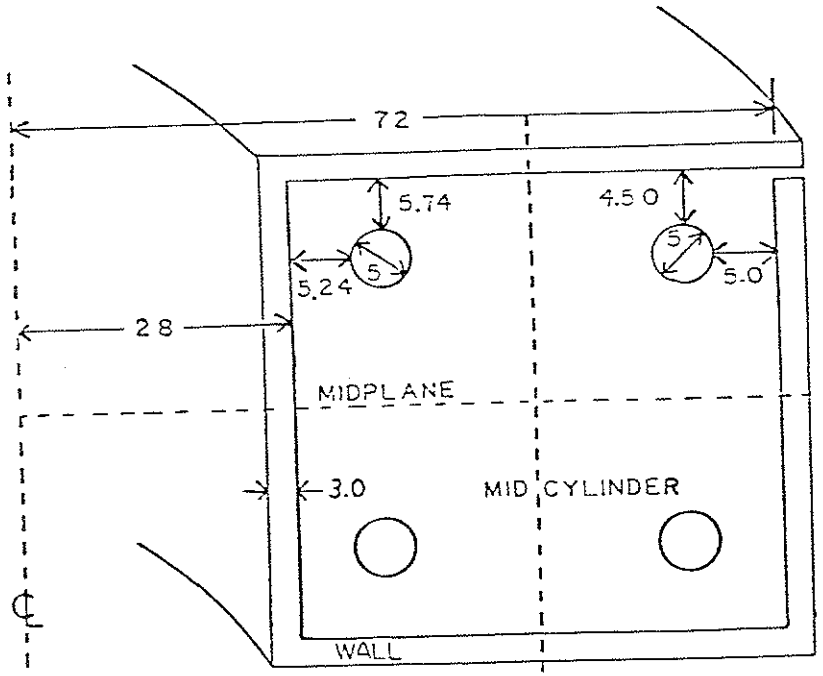

DIMENSIONS IN cm

diameter of 5 cm. Each ring is supported by three, equally spaced, high strength, beryllium-copper rods which are in turn electrically insulated from the vacuum vessel walls. The field shaping rings can be vertically adjusted ±5 mm without breaking vacuum to position the plasma.

The toroidal magnetic field, B_t, is produced by a 96 turn poloidal winding. This winding is energized by a 52 mF, 5 kV capacitor bank which is switched through a class E ignitron. The quarter period of this circuit is ~10 msec with the field passively crowbarred at peak field strength. This provides a nearly constant field for the major part of the discharge. When fully charged, this system will produce ~8 kG on the machine axis. However, due to the mechanical and electrical stresses of such high fields, the machine is normally run in the 2-6 kG range. All of the experiments described here were performed in this range.

The toroidal plasma current, I_p, and the divertor currents, I_h, in the field shaping rings are both induced by the transformer action of an iron core. The core has a flux swing capability of 0.15 webers and is usually reverse-biased ("cocked") in order to keep the core from saturating during a plasma discharge. The transformer core primary windings are driven by a 7.2 mF, 5 kV capacitor bank also switched through a class E ignitron. The 40:1 turns ratio yields a half period of ~5.6 msec. An 80:1 turns ratio is also available but not used

for these experiments. A 0.96 F, 450 V capacitor bank provides a "power" crowbar capability which clamps the poloidal gap voltage, V_{pg}, to a few volts, thus extending the discharge duration.

The poloidal field, B_p, is a superposition of the field produced by the toroidal plasma current and the vacuum octupole field generated by the four ring currents. Since these currents are in the same toroidal direction, there will be nulls (x-points) in the poloidal field located between the central plasma current channel and each of the four rings. The vacuum poloidal magnetic field is shown in Figure 3-3a, and the corresponding theoretical flux plot for a case with plasma current is shown in Figure 3-3b. Both square and dee-shaped equilibria can be produced as measured by magnetic probes[6,7]. The location of the x-points depends on the ring positions and the ratio of the plasma current to the ring currents and can be varied experimentally over a several centimeter range. The dotted line is the separatrix which represents the boundary between field lines which encircle one or more of the rings and field lines which encircle only the central plasma current channel. The plasma current is typically 10-20% of the total ring current.

The theoretical flux plot shown above assumes no plasma current flows outside the separatrix, whereas in reality roughly one-third of the total plasma current can flow in the

Fig. 3-3a: Poloidal magnetic flux plot in vacuum.

Fig. 3-3b: Poloidal magnetic flux plot with plasma.

CONTOURS OF POLOIDAL MAGNETIC FLUX

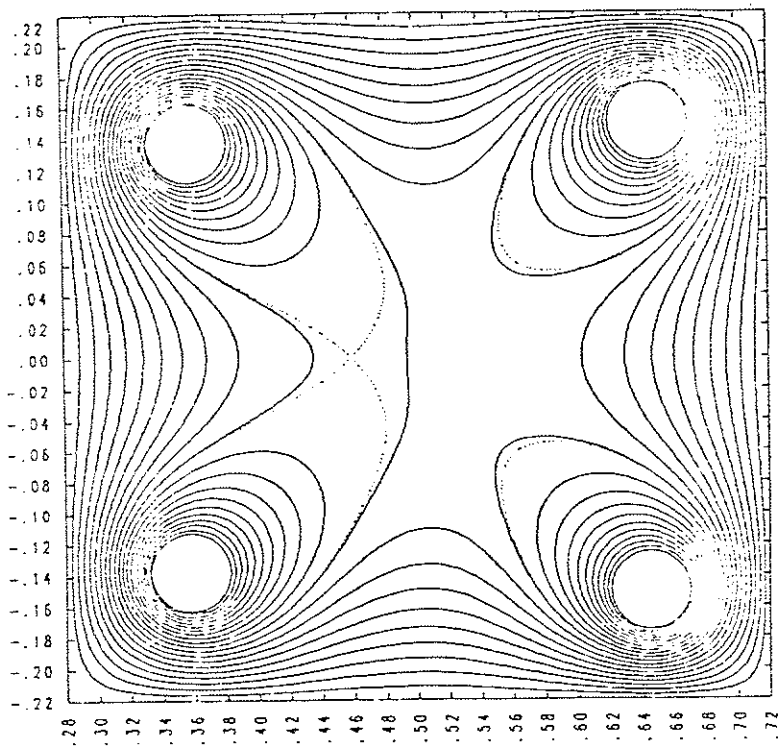

CONTOURS OF POLOIDAL MAGNETIC FLUX

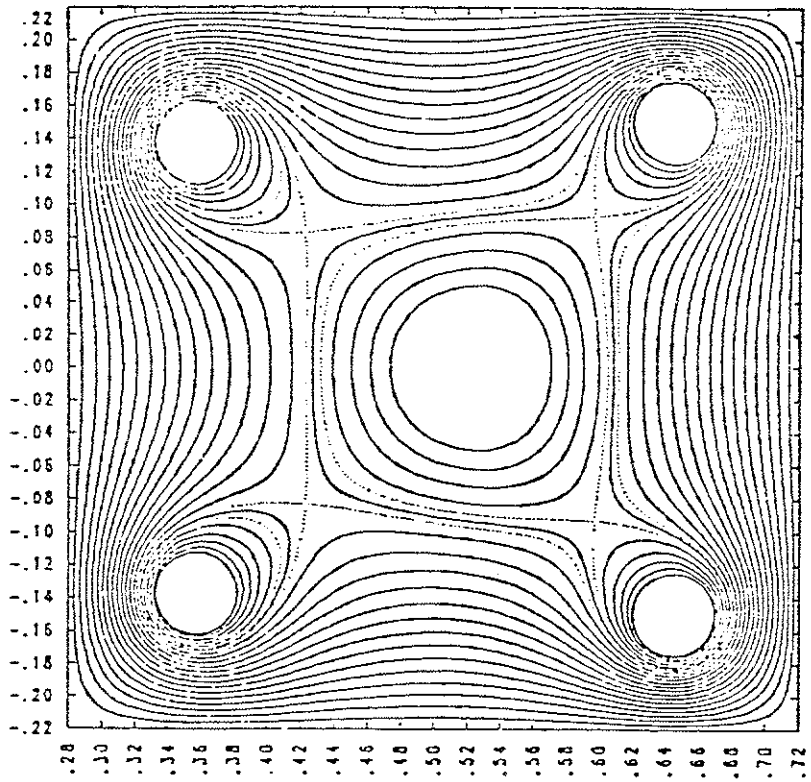

common-flux region. Stainless steel scrape-off plates can be extended up to the separatrix from all four sides at one toroidal azimuth. These "baffles" intercept field lines in the "divertor scrape-off region" and prevent current from flowing. Most of the experimental work of this thesis was done with the baffles inserted. Figure 3-4 shows the scrape-off plates and definitions for future reference.

A number of probe ports are scattered around the machine to facilitate diagnostic access to the plasma. These ports allow insertion of a wide variety of probes and diagnostics into the machine while maintaining the vessel under vacuum throughout the process.

4.B. Plasma Characteristics

Plasma formation in Tokapole II is basically the same as in all other tokamaks, and has been described in detail by Groebner[3]. For further information concerning tokamaks in general the interested reader is directed to the several review articles covering the subject[8,9,10].

The time evolution of a Tokapole II discharge is indicated schematically in Figure 3-5. A fast piezoelectric "puff" valve is triggered 16.66 msec before the poloidal gap voltage, V_{pg}, is applied, allowing hydrogen gas to fill the vacuum chamber to a pressure of typically 100-500 mTorr. The toroidal field is passively crowbarred at its peak value to provide an

Fig. 3-4: Central current channel is separated from the outer scrape-off (common flux) region by the separatrix. Stainless steel limiter plates can be inserted in scrape-off region to eliminate plasma current outside separatrix.

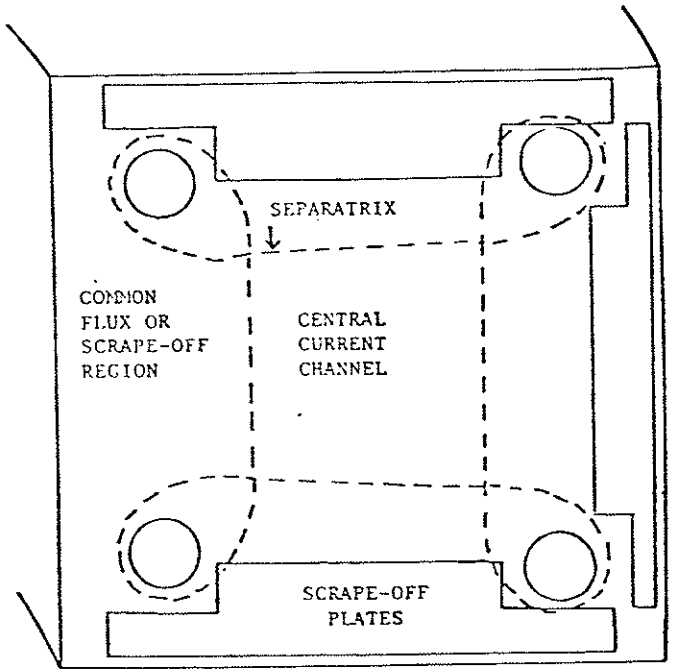

THE TOKAPOLE II DIVERTOR CONFIGURATION

Fig. 3-5: Time evolution of fields for Tokapole II discharge.

Maximum total hoop current, I_H, is typically 300 kA.

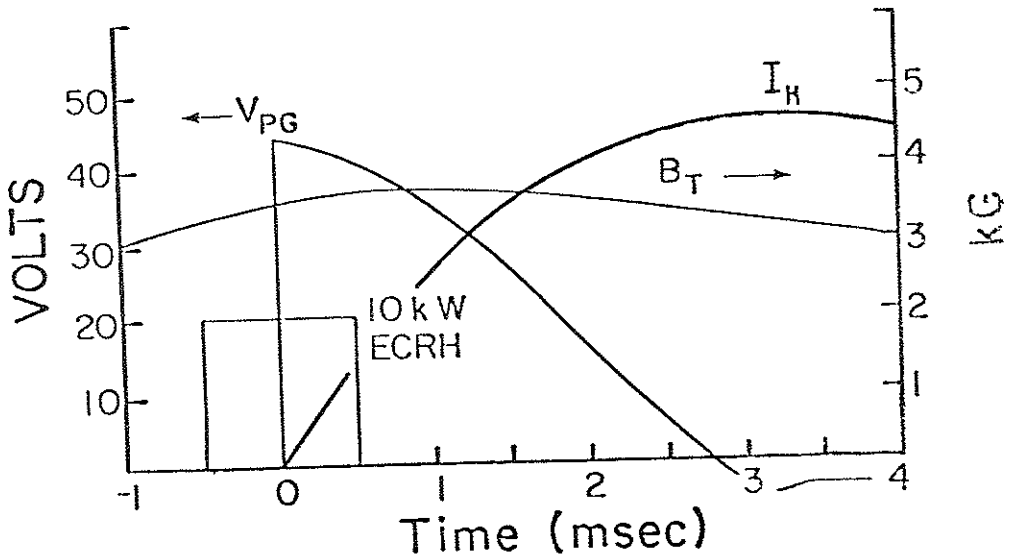
VOLTS
50
40
30
20
10
V_{PG}
I_K
B_T
10 k W
ECRH
5
4
3
2
1
kG
-1
0
1
2
3
4
Time (msec)

approximately constant toroidal field during the duration of the discharge. The poloidal gap voltage is power crowbarred to extend the length of the discharge up to a maximum of about 15 msec. Preionization is provided by 10 kW of either K-band (16.5 GHz) or X-band (9.0 GHz) microwaves depending on the toroidal field strength used. This produces a low density start-up plasma which seems to give a more reproducible discharge than would result from relying on avalanche breakdown alone.

There are two general types of discharges that have been used in these experiments. One is a relatively high current, high density discharge (but of shorter duration), while the other is a relatively lower current, lower density discharge but with a longer duration with several milliseconds of quasi-steady state (without probes inserted past the separatrix). The primary difference in the production of these two types of discharge was the presence of a "damping" resistor in the primary circuit of the transformer driving the plasma current.

Figure 3-6a,b shows current and density traces for the two types of discharge. The dashed traces are the typical results when a magnetic probe is placed several centimeters inside the separatrix. Note that the "normal" Tokapole II discharge, i.e. the longer lasting one is effected considerably more than the shorter discharge type. For considerably more detail

Fig. 3-6: Current and line average density waveforms for high current discharge (a) and for lower current "normal" Tokapole discharge (b). The dashed lines represent the typical effects of probes when inserted a few centimeters within the separatrix.

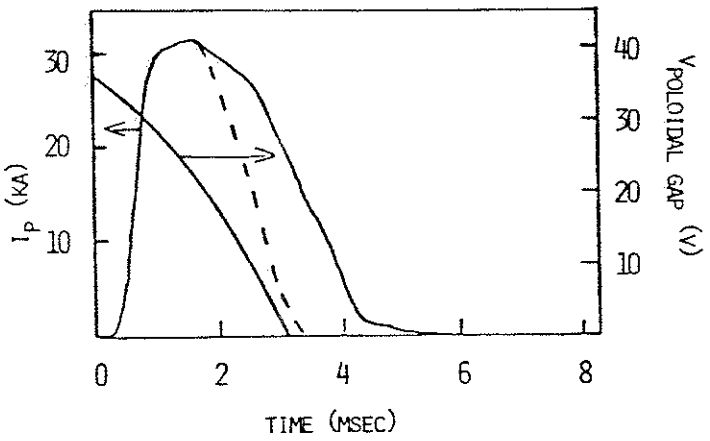
30
20
10
I_p (KA)
40
30
20
10
$V_{POLOIDAL\ GAP}$ (V)
0
2
4
6
8
TIME (MSEC)

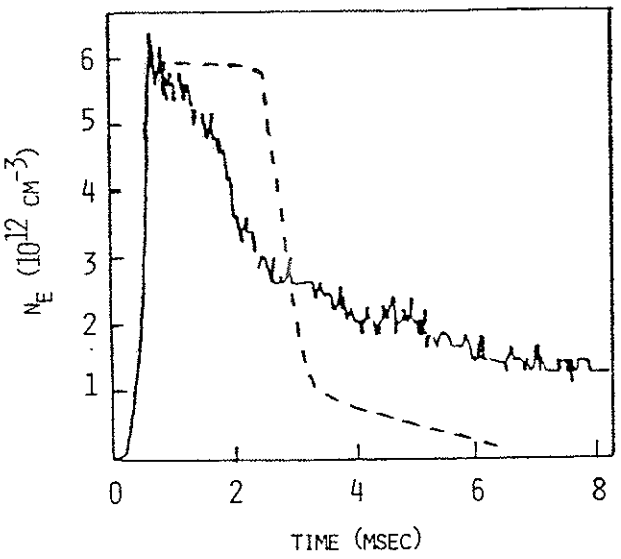
6
5
4
3
2
1
N_E (10^{12} CM^{-3})
0
2
4
6
8
TIME (MSEC)

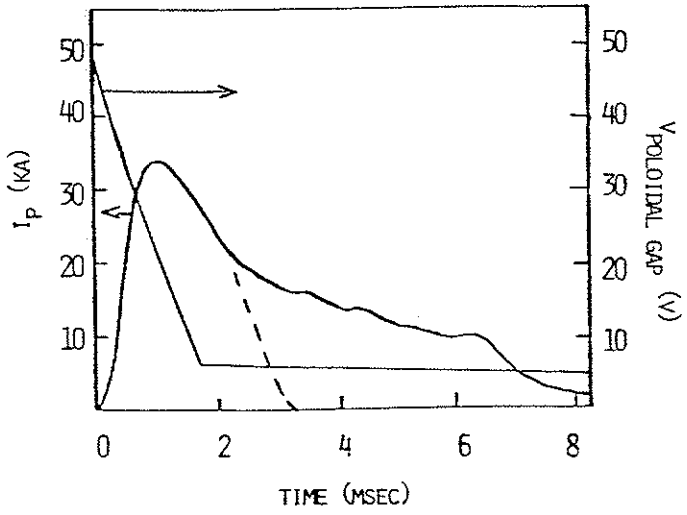
50
40
30
20
10
I_p (KA)
50
40
30
20
10
$V_{POLOIDAL\ GAP}$ (V)
0
2
4
6
8
TIME (MSEC)

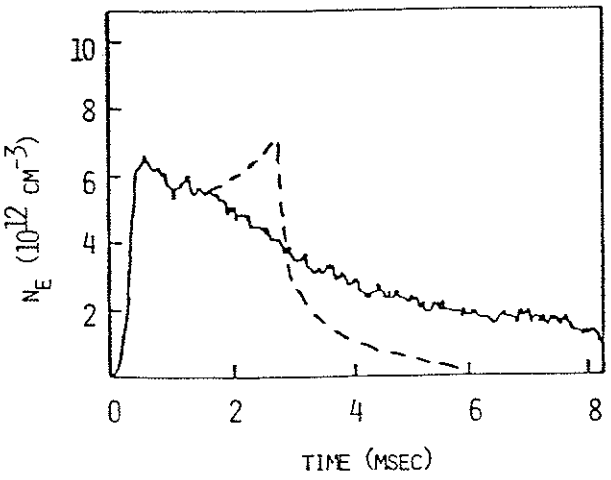
10
8
6
4
2
N_E (10^{12} CM^{-3})
0
2
4
6
8
TIME (MSEC)

concerning Tokapole II discharges, see the theses by Brickhouse[11] and Osborne[7].

Table 3-1 gives a summary of typical Tokapole II parameters.

TABLE 3.1 TOKAPOLE II PARAMETERS

Major radius	50 cm
Minor radius of plasma	6-10 cm
Toroidal magnetic field	~8 kG
Plasma current	10-40 kA
Line average density	$2\text{-}10\times10^{12}$ cm^{-3}
Electron temperature	~100 eV
Ion temperature	~20 eV
Energy confinement time	500-1000 μsec
Discharge length	3-15 msec
Base vacuum	$\sim3\times10^{-7}$ Torr

REFERENCES - CHAPTER 3

1. A.P. Biddle, et al., Nucl. Fusion 9, 1509 (1979).

2. J.C. Sprott and T.W. Lovell, University of Wisconsin PLP 744 (1978).

3. R.J. Groebner, Ph.D. Thesis, University of Wisconsin (1979).

4. L. Oren and R.J. Taylor, Nucl. Fusion 17, 1153 (1977).

5. H.F. Dylla, S.A. Cohen, S.M. Rossnagel, G.M. McCracken, and Ph. Staib, "Glow Discharge Conditioning of the PDX Vacuum Vessel," presented at the 26th National Symposium of the American Vacuum Society, New York (1979).

6. B.Lipschultz, Ph.D. Thesis, University of Wisconsin (1979).

7. T.H. Osborne, Ph.D. Thesis, University of Wisconsin (1984).

8. L.A. Artsimovich, Nucl. Fusion 2, 215 (1972).

9. H.P. Furth, Nucl. Fusion 15, 487 (1975).

10. J. Sheffield, Proc. IEEE 69, 885 (1981).

11. N.S. Brickhouse, Ph.D. Thesis, University of Wisconsin (1984).

CHAPTER 4

RF APPARATUS

4.A. Launching structures

4.A.1. Ideal launching structure

As pointed out in Chapter 2, the mode we wish to study for heating purposes is helical in nature. According to ideal MHD, the best way to drive a helical mode is with a helical antenna wrapping around the tokamak current channel with the same pitch as that of the mode. For the experiments on Tokapole II, such an antenna was completely out of the question for two reasons. First, a helical antenna would severely interfere with the many other experiments on Tokapole II. And secondly, even if there were no other experiments, it is not really possible to use a helical antenna in Tokapole II because of the divertor rings. It could not be placed outside the divertor rings because it would then link the rings, which is unacceptable for electrical reasons, and since the antenna would then be far from the plasma. Neither could it be placed inside the minor radius of the divertor rings, because proper plasma formation would then be interfered with, preventing a good equilibrium. We were thus forced to consider other possibilities.

The next best choice to a helical antenna is an array of separate and distinct loop antennas distributed about the current channel in such a fashion that, with proper phasing of the rf currents in each of the antenna loops, one obtains a step approximation to a helical antenna. The idea is illustrated in Figure 4-1. Basically, what one is doing is simply to cut out small sections of the helical antenna and then force each of these sections to carry the same current and phase it would have carried had it still been part of the original helical antenna. Obviously, the more sections used, the better the approximation to a helical antenna. But this also increases the complexity of the external driving circuitry required, since each section needs to be carefully phased with respect to the others.

In principle, if one is concerned mainly with the lowest order poloidal and toroidal modes, with mode numbers m and n respectively, then the minimum number of antennas needed for effective coupling is four. These would be distributed as two sets, with two antennas per set. Each set would be separated by 180° toroidally, and by 180° poloidally within each set. By driving these antennas either in or out of phase, one then preferentially couples to the modes (m,n)=(1,1), (1,2), (2,1), (2,2). Of course, a spectrum is actually generated, but most of the power will go into the lowest modes.

This kind of antenna system was rejected, temporarily at

Fig. 4-1: Finite section approach to a helical antenna. By operating all antennas in phase, coupling to the helical field line is obtained. Best coupling is obtained when each antenna is rotated so that it is locally parallel to the field line.

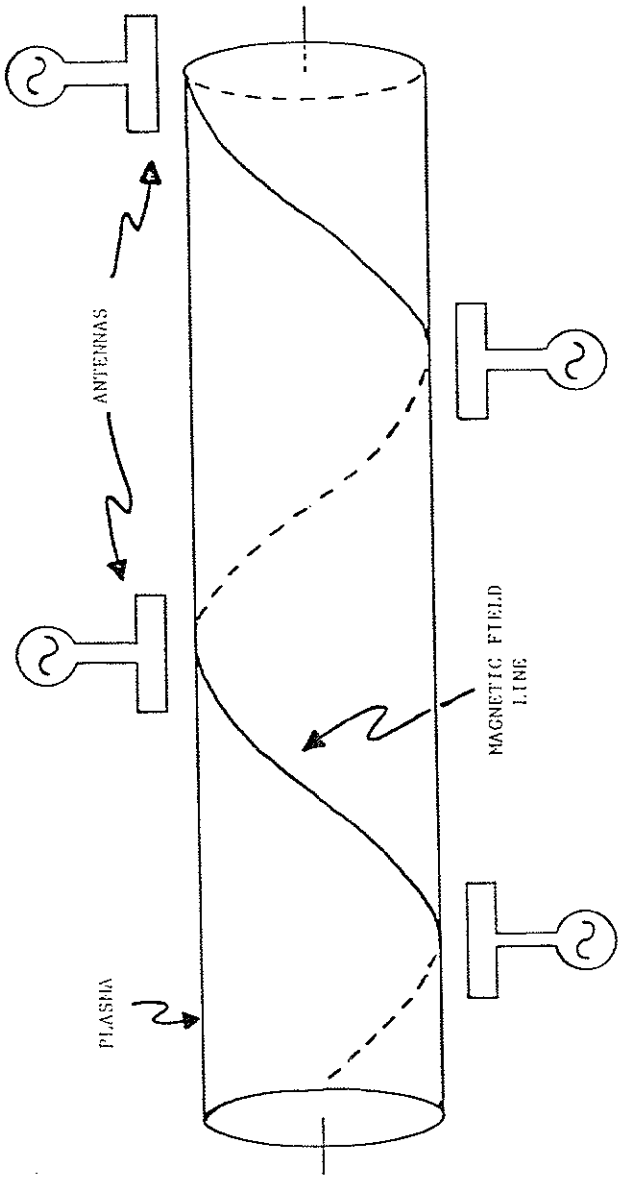

least, because it was desired to begin the experimental phase immediately, and the design and fabrication of new antennas would take some time. It was possible to make this decision at the start, because there existed another possibility for an antenna which already happened to exist. This third possibility was to utilize the divertor rings themselves as the launching structure. As will become clear, this was only an interim solution to allow experimental work to begin quickly and not the ultimately desired launching structure.

4.A.2. Divertor ring antenna

The basic idea is straightforward and is illustrated in Figure 4-2. Each divertor ring has three conducting support rods which are electrically insulated from the vacuum vessel. These supports provide the means to superpose rf currents on top of the inductively driven equilibrium "dc" currents present during the plasma discharge. What is desired is to set up an rf current distribution that has a toroidal mode structure. This can be done with the hoops simply by grounding one of the hoop supports to the vacuum vessel and driving one of the remaining supports from a source of rf power. The third support is left floating and unused in this configuration. The ring effectively acts as an inductor at rf frequencies. The resulting toroidal current distribution is plotted in Figure 4-3. Note that current flows in both toroidal directions, thus

Fig. 4-2: Toroidal mode generation of divertor ring antenna.

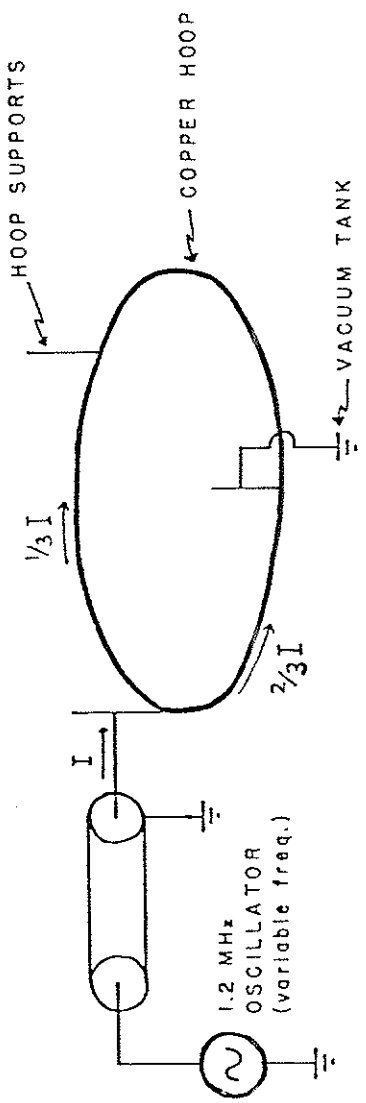

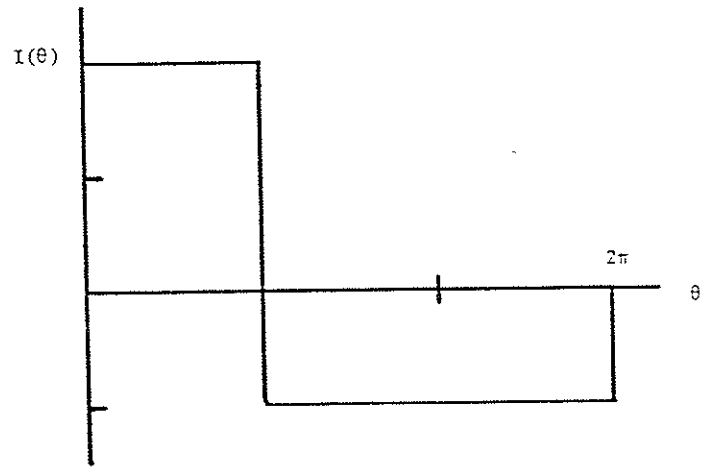

Fig. 4-3: Toroidal current distribution for divertor ring antenna. Fourier analysis yields a spectrum of toroidal mode numbers with amplitudes decreasing as 1/n. Multiples of three are absent from the spectrum due to the symmetry.

setting up a toroidal mode structure. Fourier analysis of this current distribution indicates a broad spectrum of toroidal modes but with Fourier amplitudes falling off as 1/n. Thus greater than 75% of the total power goes into the two lowest modes, n=1 and 2. Due to symmetry, mode numbers which are multiples of three are not present.

The establishment of a poloidal mode structure is indicated by Figure 4-4. For instance, an m=4 configuration is established by driving all four rings in phase with each other. Because of the geometry of the hoops, the rf currents actually fight against the helical mode for some sections of toroidal azimuth. In spite of this though, there is a weak coupling to helical modes.

There is one other method of driving the hoops which is more appealing from a symmetry point of view. That is to ground two supports while driving the remaining one. This would drive equal rf currents in opposite direction in two legs of the hoop while allowing zero current between the two grounded supports. In principle, this is a superior antenna than the single ground approach. Unfortunately, two supports cannot be directly grounded simultaneously because of the perturbations this would have on the equilibrium currents of the hoops. To get around this, we attempted to place the two supports at "ac" ground through capacitors which were a high impedance at the 100 Hz frequency of the equilibrium currents,

Fig. 4-4: Poloidal mode generation for divertor ring antenna. m=4 combination is shown. Generation of m=1 or 2 is accomplished by driving opposite rings either out of or in phase respectively.

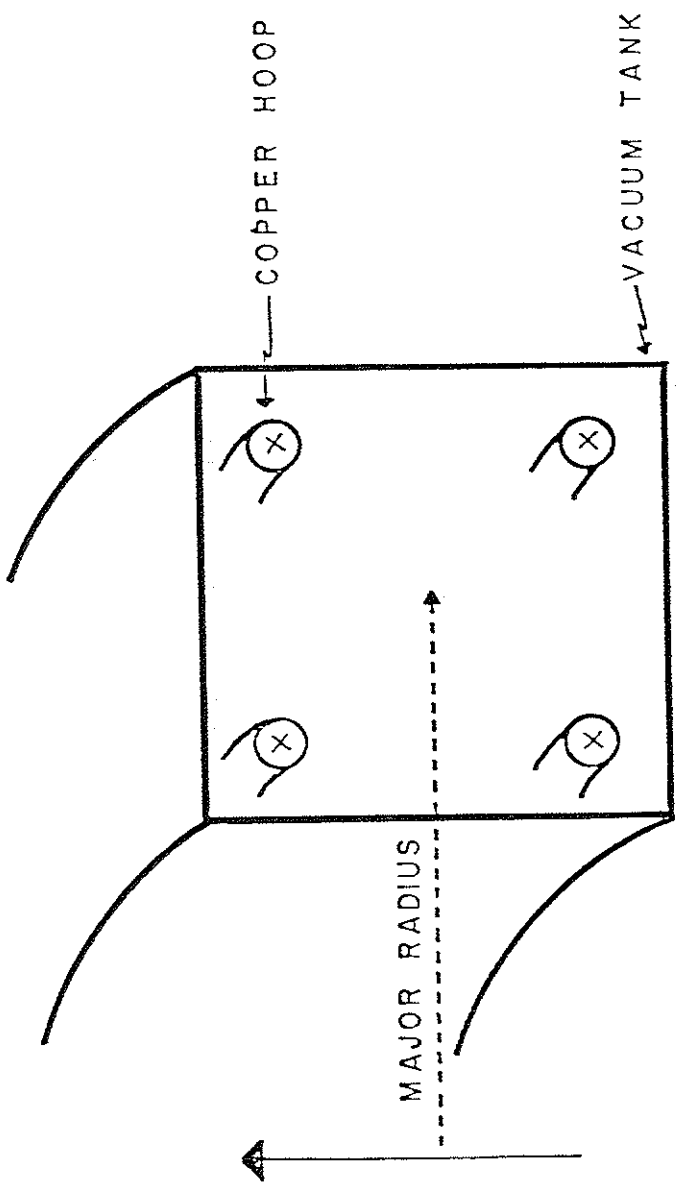

yet a small impedance at 1 MHz. This does not work very well, though, due to the extreme sensistivity of the circuit to resonant effects with the 1/3 of the ring between the "grounded" supports, and to unavoidable stray leads. It was necessary to abandon this technique for the much simpler single ground approach.

As the circuit of Figure 4-2 stands, it would be difficult to drive much rf current through the rings because of their low impedance. The situation is vastly improved by placing capacitance across the rings forming a resonant LC "tank" circuit. By choosing the capacitance to resonate the effective hoop inductance at the frequency of the rf source, the circulating current through the rings can be increased by a factor equal to the circuit Q. For the hoops this turns out to be ~20 in vacuum. This also provides a roughly constant purely resistive load to the rf source, as opposed to a low impedance inductance. The equivalent circuit for a ring is shown schematically in Figure 4-5. The equivalent circuit for an m=4 configuration is shown in Figure 4-6. At 1.2 MHz, an m=4 configuration presents a 50 Ω load to the rf source.

Probably the most serious problem encountered in this experiment has been the need to measure magnetic probe coil output signals of a few tens of microvolts in an extremely high rf noise environment. There are two approaches one can follow in trying to eliminate this noise from the measurement system.

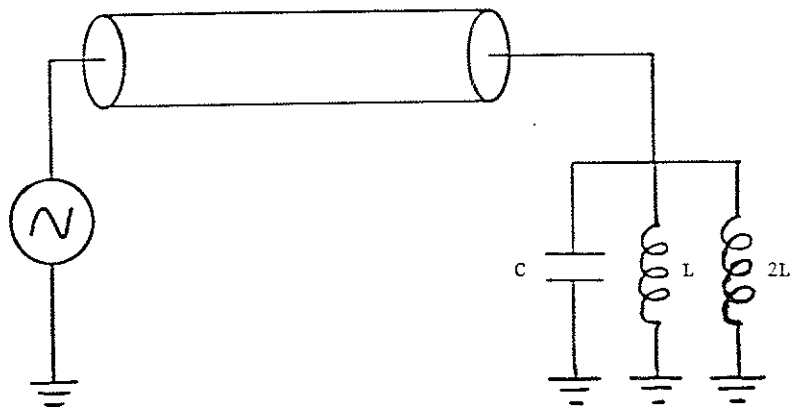

Fig. 4-5: Equivalent circuit for a single ring with resonating capacitor. L and 2L represent the inductances of the two legs of the ring.

Fig. 4-6: Equivalent circuit of m=4 configuration. Coaxial transmission lines (RG/8) from single feed line to each ring have been left out of figure for clarity.

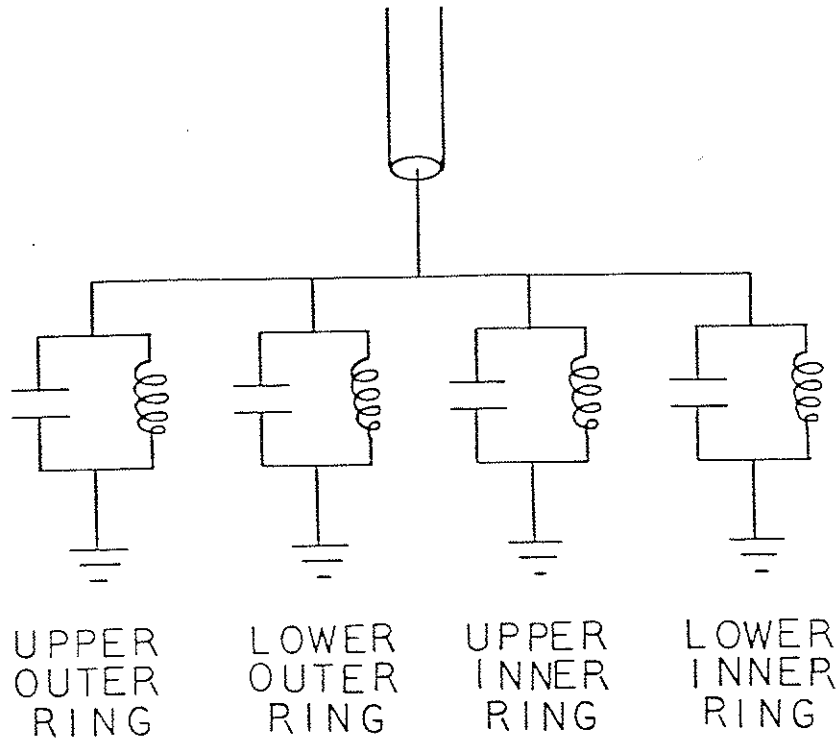

One is to shield the measurement system, which will be discussed in Section 4.C. The second is to shield the original source of the rf noise, i.e. the oscillator, transmission lines and antenna. Since neither of these techniques is 100% effective, a combined approach was found to be necessary.

Shielding the source of rf noise consists of placing an electrostatic shield around the entire rf generation system. This includes the pulse forming network, the oscillator, the transmission lines and as much of the antenna as possible. Since an antenna has the purpose of radiating rf energy, it is clear that perfect shielding is impossible. The task is to confine the rf only to the interior of this shield and thus prevent it from coupling to circuits in other parts of the room. A schematic of the arrangement that eventually worked can be found in Reference 1.

In order to avoid ground loops, which can cause as much pick-up problem as direct radiation, the electrostatic shield is grounded to the oscillator circuit ground and insulated from the Tokapole II tank which is the normal experiment ground. Copper screen mesh imbedded within a fiberglass matrix cast in the form of a "hat" covers the electrical connections to the hoops. (Schematics of this system can be found in Reference 1.) This area was identified as one of the worst radiators of the entire system due to the unavoidably large loop involved with the electrical connection to the ring supports, and due to

the proximity of this loop with its large circulating rf currents to the magnetic probes. Spurious ground loops which occur randomly can still cause significant pick-up problems if not eliminated. The rf power to the antenna is also inductively coupled from the oscillator to avoid ground loops as shown in the figure. The series resonant circuit shown in the transmission line was necessary to remove harmonic noise from the drive voltage. For more details concerning the divertor ring launching structure see Reference 1.

4.A.3. The New antenna

4.A.3.a. Reasons for a new antenna

Before describing the new antenna, let us first establish the reasons why the hoop antenna system is inadequate for future studies. These reasons provide the design rationale for the new antenna. The purpose of future studies will be focused on two aspects: more detailed study of the resonance structures and actual heating experiments. The hoop antenna system is inadequate for properly fulfilling either of these goals for the following reasons.

1) The divertor rings are not Faraday shielded and thus suffer severe electrostatic loading during a discharge due to the plasma in the private flux region around each hoop. This

lowers the Q and the parallel impedance of the resonant circuit, which are already quite low to begin with, and this in turn reduces the amount of circulating current available to drive the resonance. This reduced power delivery limits the size of the resonant magnetic field. Because of plasma generated rf noise in the frequency range that is being studied, and which cannot be filtered out without also removing the real signal, this complicates measurement of resonance properties. This has been a constant problem in this experiment, and it appears that the only solution to this particular problem is to increase the amplitude of the wave magnetic field by. Presumably, this will be possible with larger antenna current and a better coupling structure.

The original intent of the divertor scrape-off plates was to reduce the plasma near the hoops in the hope of reducing the electrostatic loading, and thus allow larger hoop antenna currents. Although the baffles succeeded in eliminating plasma current in this region, plasma density still remains quite high[2] (a few 10^{12} cm^{-3}), and electrostatic loading remains essentially unaffected. Since the parallel impedance of the hoops at resonance is very low (~50 Ω), this means the parallel equivalent impedance of the plasma would need to be quite low in order to couple significant power to the plasma. This would require at the very least a closely coupled antenna, which the hoops clearly are not.

2) A brute force approach to overcoming the electrostatic loading and low Q and $R_{\|}$ of the rings is not possible due to the low breakdown voltages that would be encountered in the ring support region when plasma is present.

3) From a physics point of view, one desires the simplest possible antenna which can excite the modes under study. The hoops have a very complicated mode structure with rf currents flowing in uncontrolled directions in the vacuum vessel walls, which act as the ground return. Not only does this complicate physics issues, but it also causes more noise pick-up problems because of the fields generated by these stray currents. As mentioned earlier, the hoops actually fight against the very modes they are supposed to be coupling to in certain parts of the toroidal extent. Obviously, this is an undesirable complication. It is highly desirable to be able to couple preferentially to either the n=1 or n=2 toroidal mode numbers without having a strong coupling to the other one at the same time. With the hoops, however, the toroidal mode structure is fixed and must be lived with.

4) One of the big questions of SARH is concerned with what is the optimal antenna (see Section 5.F). The question deals primarily with the direction of the antenna currents with respect to the ambient magnetic field (the physics of this will

be discussed in Chapter 5). To study this question experimentally requires an antenna whose orientation can be varied. The hoops do not have the capability to address this question.

5.A.3.b. Description of new antenna.

A new antenna was designed to overcome the many shortcomings of the hoop antenna and to extend the scope of possible studies at much higher power levels. The basic design follows that of the "next best design" from Section 4.A.1. A schematic diagram of the antenna is shown in two views in Figure 4-7. The antenna itself is simply a double series loop of solid copper bar. This double loop sits in a curved copper tub with the top enclosed by a Faraday shield. The purpose of the tub is to eliminate any change in inductance as the antenna is extended further into the vacuum chamber and away from the wall. This eliminates the need to retune after each antenna psoition change. It also increases the field above the antenna by roughly 50%. The Faraday shield prevents electrostatic coupling between the antenna and the plasma. The entire loop is curved to follow the toroidal direction. This keeps all parts of the antenna close to the plasma current channel and thus provides coupling over a larger plasma surface area.

The physical size of the antenna is such that it does not interfere with any future octupole studies that may be

Fig. 4-7: (a) End-on cross section view of high power antenna with representative rf magnetic field line.

(b) Schematic drawing of antenna currents indicating toroidal curvature of antenna.

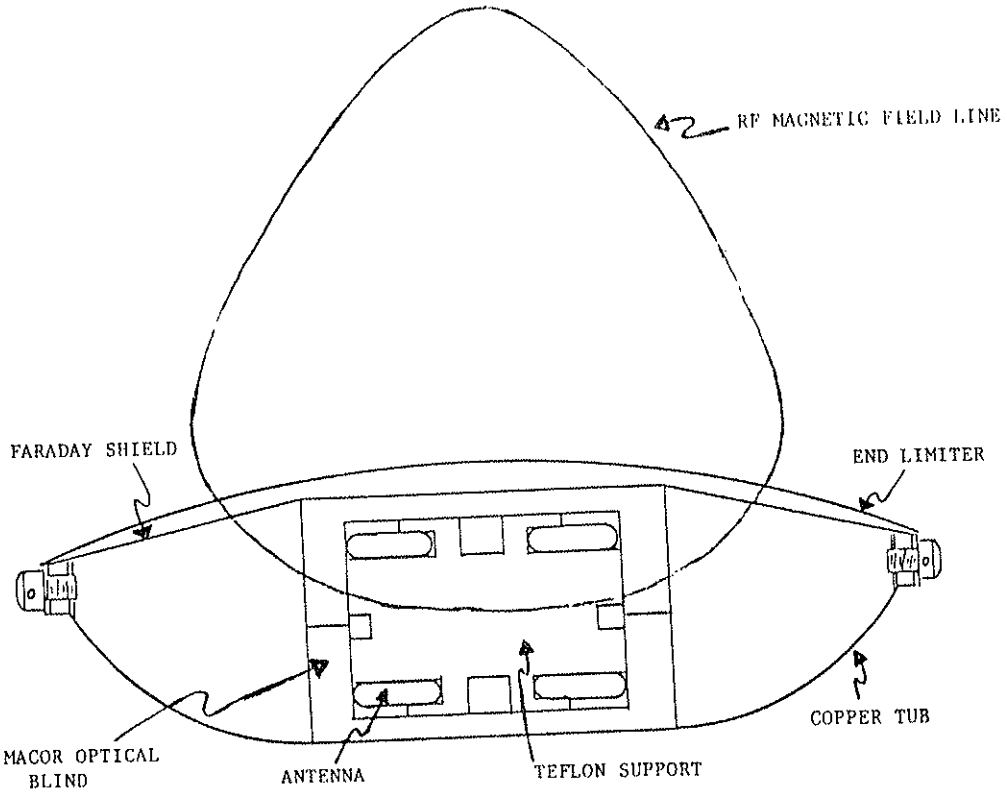
RF MAGNETIC FIELD LINE
FARADAY SHIELD
END LIMITER
COPPER TUB
MACOR OPTICAL BLIND
ANTENNA
TEFLON SUPPORT

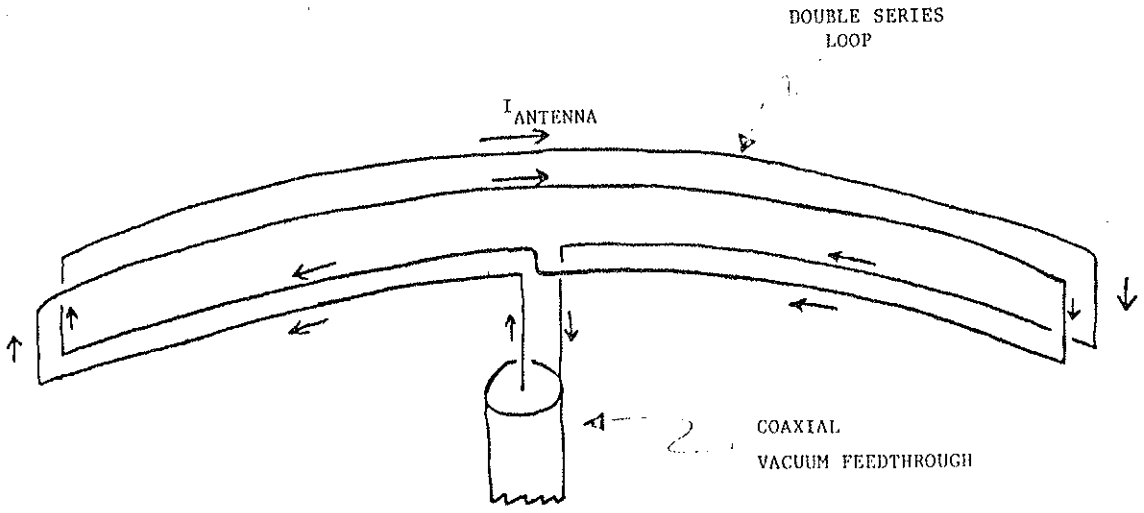
DOUBLE SERIES LOOP
I ANTENNA
COAXIAL VACUUM FEEDTHROUGH

TABLE 4.1 HIGH POWER ANTENNA SPECIFICATION

2 series loops with coaxial vacuum feedthrough

Copper Faraday shield

Antenna loops insulated from plasma with Macor

Antenna inductance	=	0.75 μH
Unshielded Q	=	155
Shielded Q	=	114
$R_{parallel}$	=	1 kΩ
Max design I_{circ}	=	2 kA
Max design V_{ant}	=	20 kV

Antenna radial insertion range = 2.25 inches

Maximum rotation range when fully retracted ±40°

Maximum rotation range when fully inserted ±15°

Toroidal extent of antenna = 54°

undertaken on Tokapole II. It thus has a fairly narrow radial width so that it can sit outside the ϕ_{crit} surface[3] of an octupole when it is not in use. Its toroidal extent is limited by the distance between successive probe ports. There is a sliding O-ring surface so that the entire structure can be radially inserted up to the separatrix. It can also rotate ±10° when fully inserted and ±25° when fully retracted. The difference is due to interference with the divertor rings. A summary of the new antenna's parameters is listed in Table 4-1. For further details see Reference 1.

4.B. RF SOURCES

This experiment has utilized a series of rf sources, gradually improving various features from one modification to the next. The first oscillator used was a single tube triode circuit with tickler coil feedback loop. The circuit diagram can be found in Reference 1. It was nominally capable of putting 100 kW into a matched load of 50 Ω. It operated at 1.4 MHz. This oscillator never worked reliably due to severe arcing problems due to its compact size, and was eventually abandoned for a larger, higher power system. It also had an unavoidable ground loop in the system because of the direct coupling to the hoops from a tapped LC "tank" inductor.

The oscillator with which most of the data in this thesis

were taken, is shown schematically in Figure 4-8. It consists of a four tube, push-push pull-pull oscillator with tickler coil feedback. Output to the antenna is transformer-coupled to the antenna to avoid the ground loop problems encountered with the first oscillator. This rf source operated typically at around 1.2 MHz, but was tunable by adjusting a vacuum variable capacitor. It was capable of delivering 130 kW to a 50 Ω resistive load, and typically generated circulating currents through the hoop antenna of 100 A in vacuum. With plasma, circulating currents were a factor of 3-4 lower due to electrostatic loading of the hoops. Voltages across the hoops were never above a few hundred volts.

When operation with the new antenna began, this oscillator was modified to an oscillator/amplifier configuration to solve mode jumping problems encountered when trying to inductively couple two high Q resonant circuits. This version of the source has driven as much as 2.0 kA of circulating current through the new antenna, and voltages of 3 kV.

All the oscillators have been powered by high voltage pulse forming networks consisting of delay lines[4]. Pulse lengths with the first source were initially 100 μsec, later extended to 250 μsec. The four tube source was run off a higher power pulse forming network than the first and provided pulse lengths of ~1.2 msec.

Fig. 4-8: Schematic of rf source.

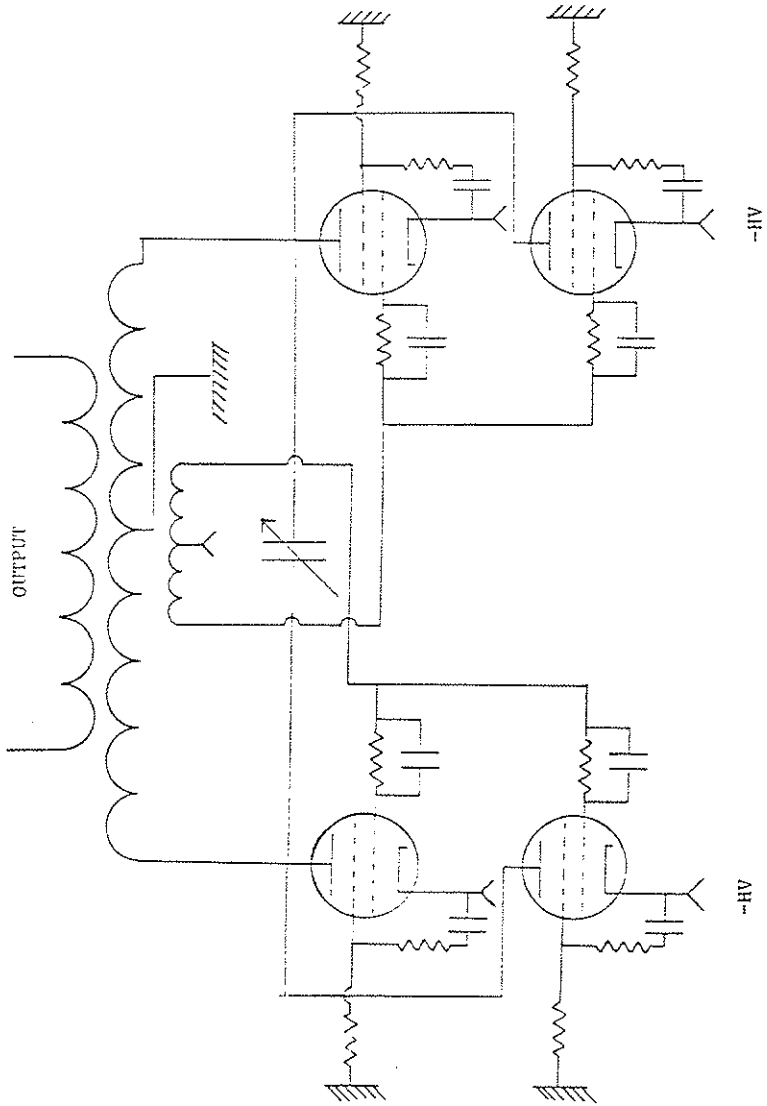

4.C. MAGNETIC PROBES

The single most difficult, frustrating, and time consuming effort in this experiment has been directed toward constructing magnetic probes[5,6,7] which meet the following three criteria. 1) The probes should have a good signal-to-noise ratio. 2) The probes should not significantly perturb the plasma. 3) The probes should survive the harsh environment of a 100 eV plasma discharge, and provide for a reliable vacuum tight seal.

Probe designs evolved in an attempt to improve each of these three criteria. This was by no means an easy task, and is described in more detail in Reference 1. In this section we will describe only the final conclusions of this developmental effort. Those conclusions are:

1) The solution to the first criteria turns out to be two-fold. First, the probe design must include a complete electrostatic shield enclosing the pick-up coils and the associated electronics. Secondly, the rf source, transmission lines and antennas must be properly shielded to reduce the origin of the rf "noise" to begin with. This was already dealt with in a previous section. A schematic of the rf shielding system used around the probe and the associated electronics is shown in Figure 4-9. This entire shield is connected to Tokapole II ground at one single point on the vacuum vessel wall near where

Fig. 4-9: Magnetic probe shielding system and electronics.

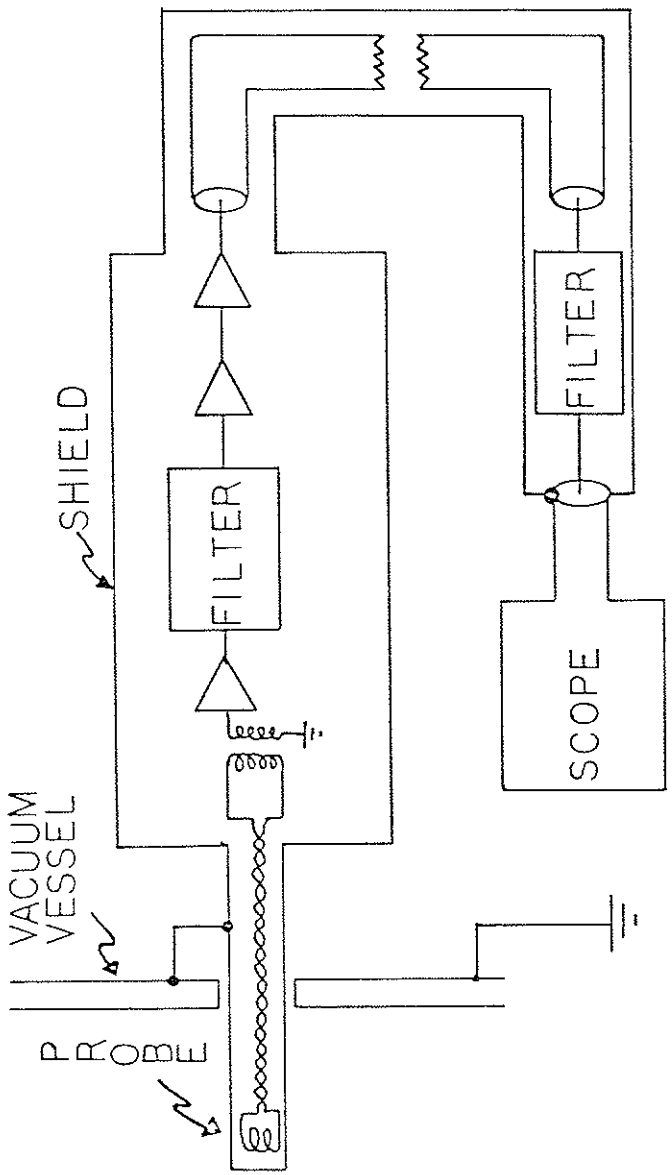

the probe enters the vacuum vessel. Oscilloscopes are floated with respect to power line ground.

2) Plasma perturbations cannot be entirely eliminated for any of the normal Tokapole II discharges. (Probes seem to have very little effect on extremely low current (<5 kA) low temperature discharges as would be expected.) For an indication of probe effects on the discharge see Figure 3-6. The only answer here is to try to reduce the perturbations to a minimal level. There are two primary techniques to achieve this. One is to utilize the physically smallest probe possible. This reduces the surface area exposed to the plasma, and thus reduces the impurity "boil-off" which causes perturbations in the local resistivity which in turn reduces the local current density. The second technique is to utilize probe tube materials which are not easily sputtered and also consist of only low-Z constituent atoms. Low-Z atoms reduce the local cooling effects due to ionization of the impurities released from the probe tube.

3) One cannot choose arbitrarily small probe dimensions. The inner bore of the tube must be large enough to accomodate a reasonably sized magnetic pick-up coil. Also, as probe dimensions get smaller, it becomes more susceptible to thermal shock and less able to dissipate the absorbed heat load. The

material of the probe tube must have a very high melting point. Most ceramics, like Alumina, which have high melting points, cannot take the thermal shock and other mechanical stresses of the pulsed Tokapole II environment.

The probe design that represents the compromise solution to all these requirements is shown in Figure 4-10a. The 1/4" tube acts only as a mechanical support structure for the less rigid 5/32" tube which actually extends into the plasma. Tubes smaller than 5/32" turn out to be unsatisfactory since the thicker walls reduce the inner bore to such a small size that reasonably sized magnetic coils cannot be inserted within the tube. Thinner walls which do allow a larger bore size, consistently have their tubes destroyed by the discharge causing serious vacuum accidents and coil destruction.

This probe had to be used very carefully to avoid its destruction. Discharge cycle rates were kept very low (~ 12-15 per hour), with periodic (1 per hour) "cool-down" periods to keep from overheating the tube tip. But even this was not sufficient to prevent probe destruction. It was found to be necessary to rotate the probe tube 90° after each plasma discharge. This "barbecue mode" served to spread the heat load over a wider area to prevent local melting due to the low thermal conductivity of stainless steel. These operating procedures did not prevent probe damage; they merely reduced it

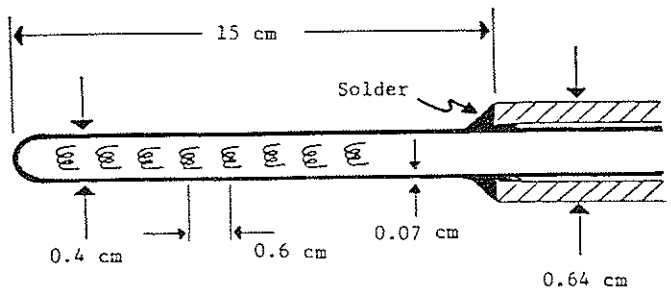

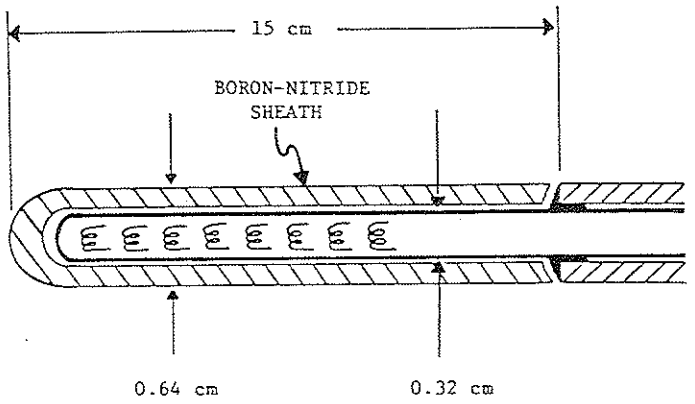

Wall thickness 0.025 cm

Fig. 4-10. (a) Stainless steel tube magnetic probe.

(b) Boron-nitride sheathed magnetic probe.

to a level that prolonged tube life enough to allow a tube to be used for several runs before requiring replacement.

To achieve the minimum plasma perturbations, the probe needs extensive conditioning. This consists essentially of scouring the probe tube in a plasma discharge. The tube is constantly maintained under vacuum in the probe port even when not being used, to avoid coating the surface with atmospheric impurities such as oxygen and water. The tube is also placed into the glow discharge[8] cleaning plasma overnight for many nights. At the start of a run period the tube is then inserted into the discharges and slowly scoured for a period of typically 2 hours. As the tube surface cleans up, the disturbance of the plasma discharge become somewhat less. There is always a minimum perturbation beyond which no amount of cleaning seems to help. The plasma current waveforms shown in Figure 3-6 were for the least perturbing probes after extensive conditioning. Without this conditioning, the perturbations are considerably worse.

In addition to the extreme care required for the probe tube, great care also must be exercised with the coils inside. These coils cannot be left at the tip of the probe continuously. Because of the high temperature of the tip after just a few discharges, the coils and the coil forms inside would get too hot, melting the Teflon coated wire insulation and causing the coil to stick to the tube wall, and eventually

shorting to the wall. Thus the coils had to be withdrawn from the tip after each discharge, removing it from the heat source, and then reinserted moments before the discharge trigger. This method allowed coils to last longer than the tubes.

Most of the problems associated with probe tube design have recently been solved by a newer approach. This design is shown in Figure 4-10b. It consists of a 1/4" O.D. boron-nitride sheath[9] machined out of solid rod which is bonded to a 1/8" stainless steel tube. Although the boron-nitride sheathed probe has a larger outer diameter than the 5/32" stainless steel tube, it has proven to have somewhat less of a perturbation to the plasma probably because of its low-Z composition. It appears to have completely solved the problem of probe and coil destruction. The boron-nitride sheath has survived the highest current and hottest discharges in Tokapole II with no significant damage. The only drawback is its small mechanical strength. It will break under small stress. This has proven not to be a serious drawback though. Heat load to the coils inside has been drastically reduced as indicated by thermocouple measurements inside the tube[1]. Thus coils can be left in place between shots. This design is now the standard magnetic probe design used for all magnetic field measurements on Tokapole II. In addition, reproducibility of the plasma discharge with this probe inserted seems to be much better than with stainless steel probes.

REFERENCES - CHAPTER 4

1. F.D. Witherspoon, University of Wisconsin PLP 921 (1984).

2. T.D. Rempel and G.A. Emmert, University of Wisconsin PLP 894 (1983).

3. R. Dory and T. Cook, University of Wisconsin PLP 5 (1962); R.L. Willig, University of Wisconsin PLP 20 (1963).

4. C.M. Fortgang, University of Wisconsin PLP 826 (1980).

5. R.H. Lovberg, in Plasma Diagnostic Techniques, eds. R.H. Huddlestone and S.L. Leonard (Academic Press, 1965) Chapter 3.

6. S.E. Segre and J.E. Allen, J. Sci. Instr. 37, 369 (1960).

7. R.H. Lovberg, Ann. Phys. 8, 311 (1959).

8. H.F. Dylla, S.A. Cohen, S.M. Rossnagel, G.M. McCracken, and Ph. Staib, "Glow Discharge Conditioning of the PDX Vacuum Vessel," presented at the 26th National Symposium of the American Vacuum Society, New York (1979).

9. P.D. Coleman, B.D. Blackwell, M. Kristiansen, and M.O. Hagler, IEEE Transactions on Plasma Science, PS-9, 123 (1981).

CHAPTER 5

EXPERIMENTAL RESULTS AND DISCUSSION

This chapter presents data which we believe constitutes a clear identification of the shear Alfvén resonance in a tokamak. We will present this data in a topical format, first describing the general properties of the resonances: i.e. polarization, radial width, risetime, and resonant enhancement factor, and comparing these with the MHD theory presented in Chapter 2. In the last section, we will compare the measured radial location of the resonances with the predictions of the 2-D theory discussed at the end of Chapter 2.

The bulk of the data has been obtained with the divertor ring antenna system. However, initial results from the new antenna have provided some significant complementary data which serve to strengthen the validity of the ring antenna results. Since we follow a topical approach, data from both launching structures will be presented together throughout the chapter. The next chapter will give a summary of the results and some suggestions for future studies.

5.A. General Radial profile

Let us first consider what a typical experimental resonance looks like, and then go on in the following sections

to discuss each of the particular properties of the resonance in more detail. Figure 5-1 shows a typical radial profile of the poloidal wave magnetic field generated by the divertor ring antenna. This profile was obtained with a single-coil magnetic probe with the tip of the probe tube placed 3.0 cm out from the center of the vacuum vessel (on the mid-plane), and then moving the internal coil to different radial locations on each successive plasma shot.

There are a few general features of these profiles that bear discussion. The most obvious characteristic is their double-peaked nature. This is a general feature of profiles obtained with the divertor ring antenna, which is in marked contrast to the profiles generated so far by the new Faraday shielded antenna (hereafter referred to as the Alfvén antenna). A typical profile produced by the Alfvén antenna is shown later in the chapter in Figure 5-10. It indicates only a single resonance deep inside the current channel, with no peaking outside the separatrix. To date, no resonance has ever been observed outside the separatrix with the Alfvén antenna.

Our interest is primarily focussed on the resonance within the separatrix, since this is the one that would be used for heating in a tokamak reactor. The outer resonances are not as reproducible as the inner ones, both in size and location. Thus, we have not investigated them to the same extent as the inner ones.

Fig. 5-1: Representative radial profile of poloidal wave magnetic field taken along horizontal mid-plane.

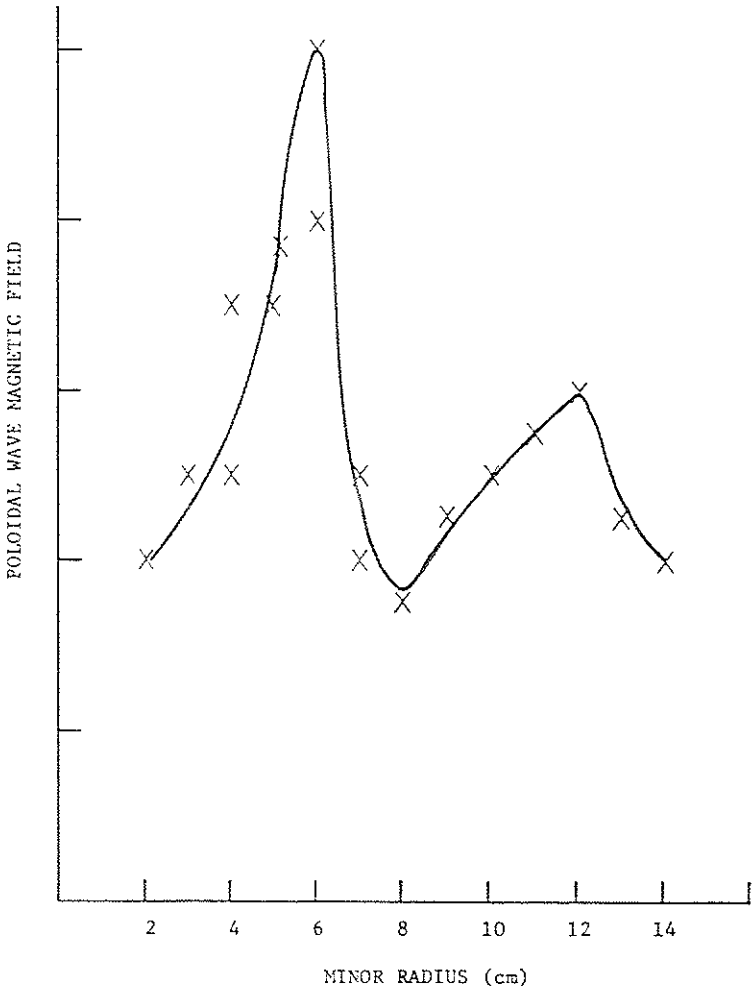

The dip in the profile always seems to occur either at, or at least very close to, the position of the separatrix as calculated by the equilibrium code. This is exactly what would be expected for shear Alfvén waves based on the screw-pinch model. Recalling Equation 2.14

$$\omega^2(r) = (n + \frac{m}{q})^2 \frac{B_\phi^2}{\mu_o \rho R^2}$$

we note that at the separatrix the safety-factor, $q \to \infty$. This has the effect of removing the mode number, m, from the expression, leaving the resonance frequency to be determined by the toroidal mode number, n. Since the SARH technique typically requires mode numbers of opposite sign to obtain low frequency solutions, we find that at the separatrix, only very much higher frequencies have solutions. For the frequencies at which we operate, 1.0-1.4 MHz, we are below the lowest such frequency; for n=1, the lowest frequency is about 2.0 MHz.

It is not particularly surprising that the Alfvén antenna doesn't produce an outer peak. Since the fields and density are sufficient to support shear Alfvén waves in this frequency range and since this resonance is polarized perpendicular to the field, it seems likely that this outer resonance is some manifestation of a local Alfvén wave. However, we do not at present know whether these are global modes in the same sense as the resonances within the separatrix are. If it is indeed

an Alfvén wave, the small coupling to this region due to the finite extent of the Alfvén antenna, as compared to the global extent of the divertor ring antenna is probably the reason no outer resonance is seen with the Alfvén antenna. When all four Alfvén antennas are installed, coupling may become strong enough for it to reappear.

5.5. Polarization

As we discussed in chapter 2 for the screw-pinch model, $b_\parallel \sim \sin\omega_0 t$, and thus remains finite at the resonance. However, $b_r \sim \ln t \sin\omega_0 t$ and $b_\perp \sim t \sin\omega_0 t$ at the resonance. Thus, both the radial component and the perpendicular component which also lies in the flux surface blow up at the resonance, with the perpendicular component being much more strongly divergent. This is clearly illustrated by the polarization plot of Figure 5-2. Here, we see that the wave field is indeed polarized perpendicular to the equilibrium field direction (which is mostly toroidal), indicated by the dashed line. This plot was obtained from a resonance produced by the Alfvén antenna. This is consistent with polarization measurements of resonances generated by the hoops, for which the ratio b_{pol}/b_{tor} of the wave fields is typically 7-10, the aspect ratio of the device.

Figure 5-3 shows a radial profile of the radial component of the wave field, b_{radial}. This profile was taken for the same case as shown in Figure 5-1, but somewhat later in the

Fig. 5-2: Polarization plot of resonance shows resonance polarized perpendicular to the equilibrium magnetic field indicated by dashed line.

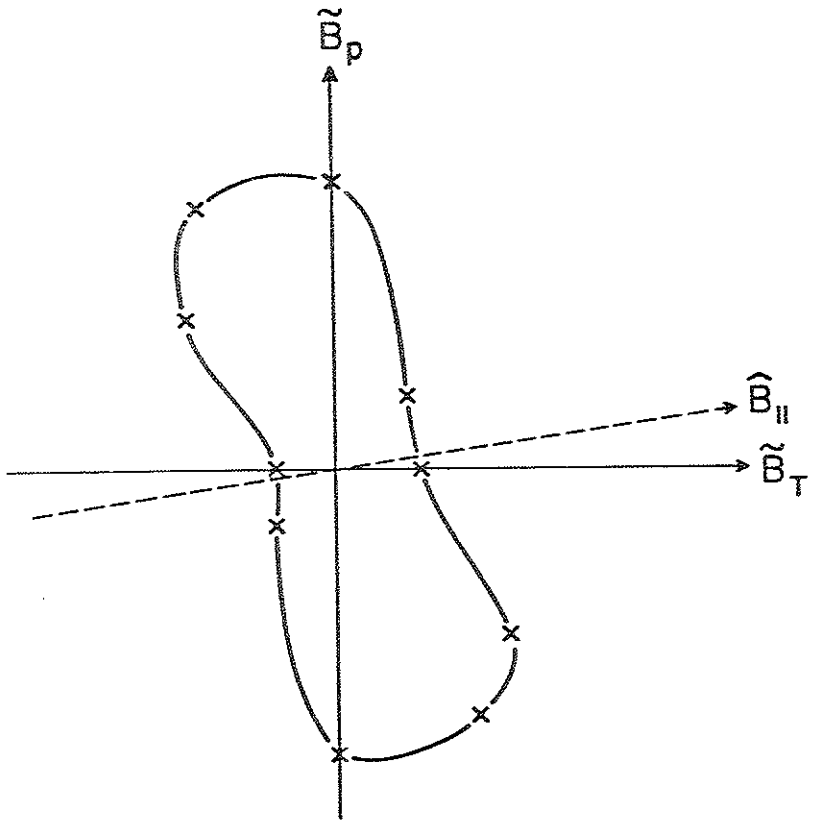

Fig. 5-3: Radial profile of radial wave magnetic field.

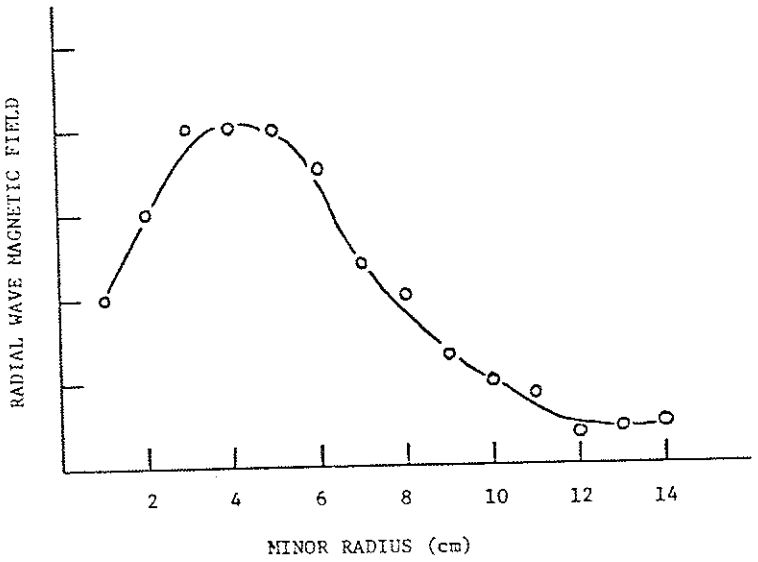

run. As predicted by theory, the maximum amplitude of this field is smaller than that of the poloidal signal. It is also interesting to note that the resonance in b_{radial} does not occur at the position of the outer peak.

5.C. Radial width

Ideal MHD theory predicts that as $t \to \infty$ not only do the fields blow up, but the radial width of the resonance, Δ, approaches zero. However, just as dissipation of the wave field energy prevents the wave fields from becoming infinite, so too does it keep Δ finite. The resistive MHD estimate for Δ is given by Eq. 2.16

$$\Delta = 8\pi\left(\frac{\eta}{\mu_o\omega_o}\right)^{1/3}\left(2\frac{B'}{B} - \frac{\rho'}{\rho}\right)^{-1/3} .$$

This expression has been solved for Tokapole II discharges, and is plotted in Figure 5-4 as a function of the logarithmic derivative of the density profile, with the resistivity acting as a parameter through its dependence on T_e and Z-effective. The most probable regime for Tokapole II discharges is indicated by the cross-hatched region, indicating that the most probable value for the radial width due to ohmic dissipation is in the range 4.0-8.0 cm.

Experimentally, typical resonance widths range from 2.0 cm

Fig. 5-4: Predicted width of resonance due to ohmic dissipation. Parameter regime for Tokapole II indicated by cross-hatched region.

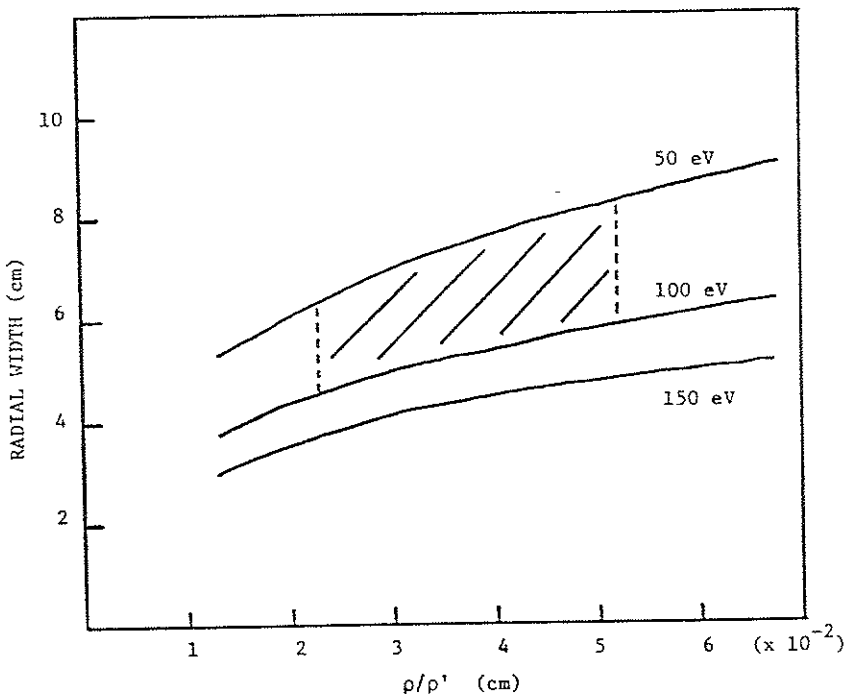

up to 5.0 cm. The narrowest resonances have been observed with the 8-coil probes, as would be expected, since this eliminates broadening due to shot-to-shot variability of the plasma discharge. A good example of such a single shot resonance is shown in Figure 5-5. Resonances generated by the Alfvén antenna have widths comparable to those generated by the divertor rings, being typically about 5.0 cm in width. See Figure 5-10.

We can also make some rough estimates of the radial width due to other dissipative mechanisms such as electron Landau damping and ion viscosity. Using Eq. 2.18 we find that the width due to ion viscosity is negligible compared to the ohmic width. From Eq. 2.19, we find that the width due to electron Landau damping is roughly a factor of four larger than the ohmic heating width. It should be noted that the electrons for Tokapole II are in the plateau region of collisionality.

5.D. Risetime

From chapter 2, we saw that dissipative processes prevent the wave fields from growing indefinitely. The fields will grow linearly at first, but then saturate as energy is dissipated by the plasma as fast as it is being delivered by the external source (i.e. the antenna and rf source).

The resistive MHD calculation discussed in Chapter 2 also

Fig. 5-5: Resonance profile obtained with 8-coil probe on single shot.

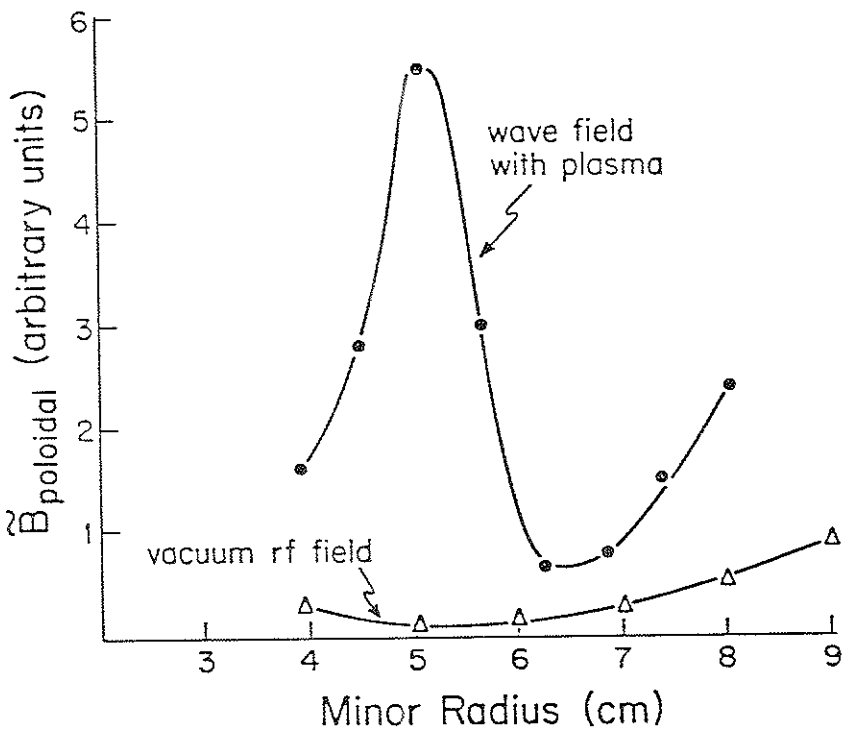

gave an estimate of the risetime due to ohmic dissipation. The expression is given by Eq. 2.15

$$\tau_{rise} = \left(\frac{24\mu_o}{\omega_o^2 \eta}\right)^{1/3} \left(2\frac{B'}{B} - \frac{\rho'}{\rho}\right)^{-2/3} .$$

This function is plotted in Figure 5-6. The cross-hatched region is the most probable parameter regime for Tokapole II discharges, indicating a probable risetime of 4-9 μsec.

Determining the experimental value for the risetime is difficult. If the resonant risetime is much faster than the risetime of the external driving rf antenna currents, then only an upper bound can be placed on the resonance risetime. This is the case for our experiment. The risetime of the circulating currents in the antenna to their steady state value places an upper bound of roughly 40 μsec on the resonant risetime.

5.E. Resonant enhancement of wave amplitude

One of the important features of the SARH technique is that the amplitude of the driving wave is enhanced to a large value at the resonance. For reactor grade plasmas, Hasegawa and Chen[1] has estimated that the enhanced value of the wave field could be as much as 100 times the driving vacuum field at the same location. The importance of this feature is that one does not need to drive such large vacuum magnetic field

Fig. 5-6: Predicted risetime of resonance based on ohmic dissipation. Parameter regime for Tokapole II indicated by cross-hatched region.

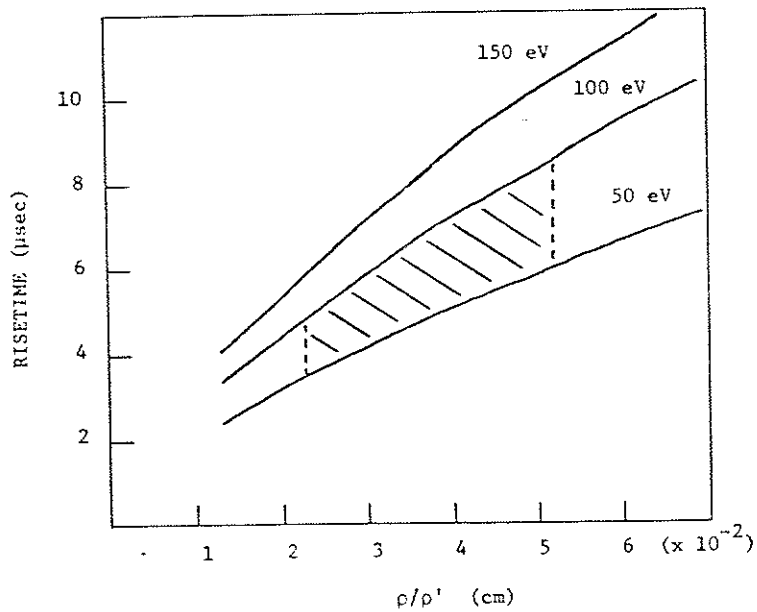

strengths, but can allow the plasma to resonantly enhance the wave fields to a higher value where non-linear damping processes can occur such as coupling to the ion-acoustic wave and its subsequent damping.

An expression for this enhancement ratio was given in Eq. 2.17

$$|B_{pol}| = (\kappa\rho_i)^{-2/3}(1 + \frac{T_e}{T_i}k_x^2\rho_i^2)|B_{pol\ vac}|$$

Figure 5-7 shows calculated values for the enhancement factor for three different ratios of T_e to T_i. The best estimate for Tokapole II is within the dashed lines predicting an enhancement ratio in the range of 30-50. Experimentally, the enhancement factor ranges from 20-50 for the inner peaks and considerably less for the outer peaks (<5).

To calculate properly the enhancement factor for the new antenna, really requires a more complete set than the single antenna now installed, since the theoretical calculation assumes a global antenna. We would thus expect that a single antenna "point" source such as now exists would not have such a large enhancement factor since power is being put into the mode at only one locality. Measurement of the fields immediately above the Alfvén antenna indicates a ratio of 5-10. Ratios measured at other toroidal azimuths naturally are much larger, since the effective forcing field there is negligibly small.

Fig. 5-7: Resonant enhancement factor of resonant wave fields over corresponding vacuum wave fields. Parameter regime for Tokapole II is within the dashed lines.

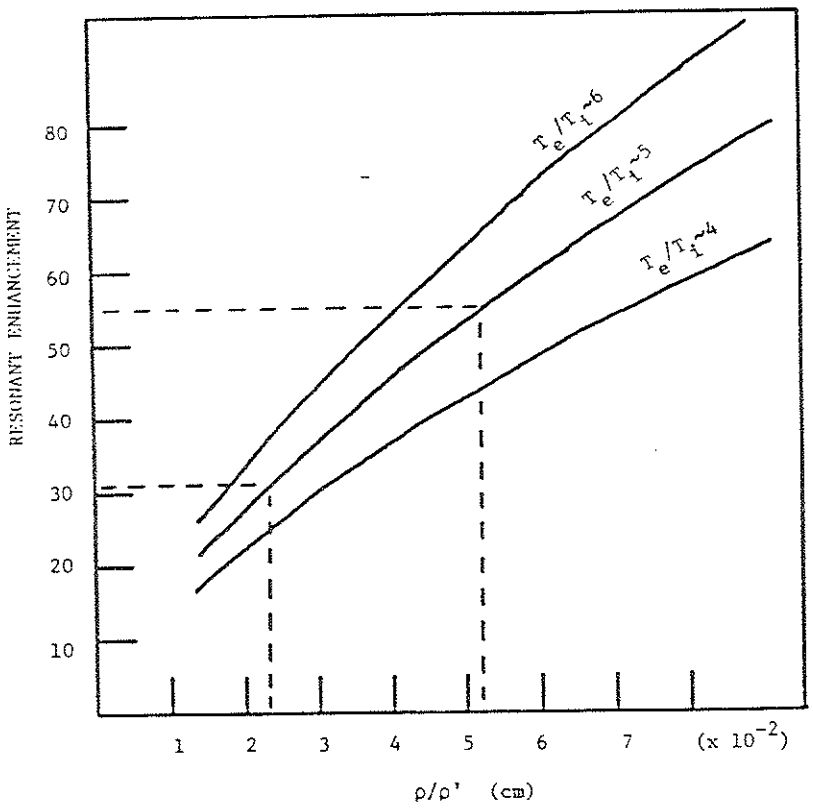

We thus consider these numbers as inappropriate. As more antennas are installed, and more power is coupled into the modes, but with the local forcing fields above each antenna remaining the same, we expect this ratio should approach the expected value, as for the rings.

5.F. Loading

A fundamental measurement in rf heating experiments is the loading of the rf system due to coupling to wave modes in the plasma. Usually, the interaction is modelled as a complex impedance, representing the plasma, in parallel with an LC circuit, representing the antenna. As coupling becomes stronger, the equivalent plasma impedance becomes smaller, loading down the parallel impedance of the antenna circuit. If the coupling is very small, then the effective parallel impedance of the plasma is much larger than the parallel impedance of the LC circuit, which is just a pure resistance at resonance. Any imaginary part of the plasma effective impedance serves to detune the LC circuit off resonance. This can be compensated by tuning the drive frequency off resonance and allowing the plasma to "pull" the LC circuit into resonance.

Thus, as coupling to a mode becomes stronger, the effective parallel impedance of the LC circuit is reduced, which means the circuit Q is reduced, and the circulating

current through the circuit is reduced. Thus, monitoring the circulating current and voltage across the LC circuit is a good way of determining when there is coupling between antenna and plasma. A more detailed explanation of this has been given by Fortgang[2].

Consider then that for a brief period during the discharge, the proper conditions arise for coupling between the antenna and a shear Alfvén mode in the plasma. This could arise as a result of the evolution of the discharge, e.g. the density or the plasma current changing with time. As this resonance condition first appears and then disappears, one would expect to see a dip in the circulating current through the antenna. Its width in time would, of course, depend on how fast this resonance condition was swept through.

We have looked for evidence of such effects in this experiment. With the hoops, this is very difficult to do because of the severe electrostatic loading of the hoops and because the effect is so small due to the weak coupling of the hoops to the shear modes. In spite of this, however, we have been able to observe the effect. One such case is shown in Figure 5-8 (a) where we show a trace of a probe signal measured at the peak of the resonance, and at bottom a trace of the circulating current through one of the hoops, in this case the upper outer hoop. During the time when the probe signal goes to zero, indicating the brief disappearance of the resonance,

Fig. 5-8: (a) Upper trace: poloidal wave field on resonance. Bottom trace: circulating current through upper outer ring.

(b) Upper trace: poloidal wave field on resonance. Bottom trace: circulating current through high power antenna. Both traces on same time scale even though picture sizes are different.

POLOIDAL WAVE MAGNETIC FIELD ON RESONANCE

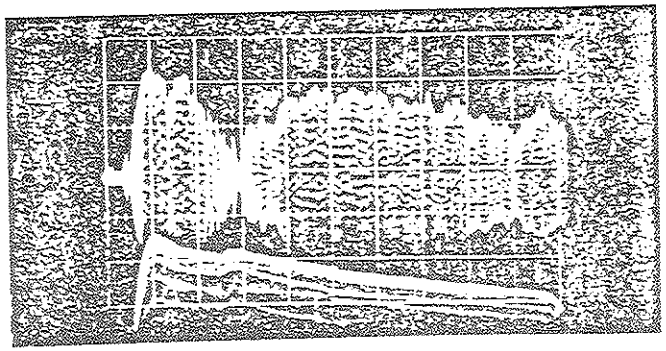

CIRCULATING CURRENT THROUGH UPPER OUTER HOOP

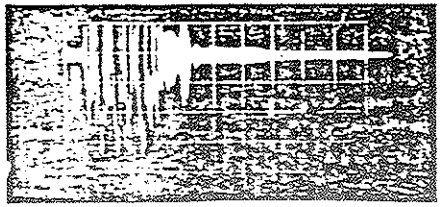

POLOIDAL WAVE MAGNETIC FIELD ON RESONANCE

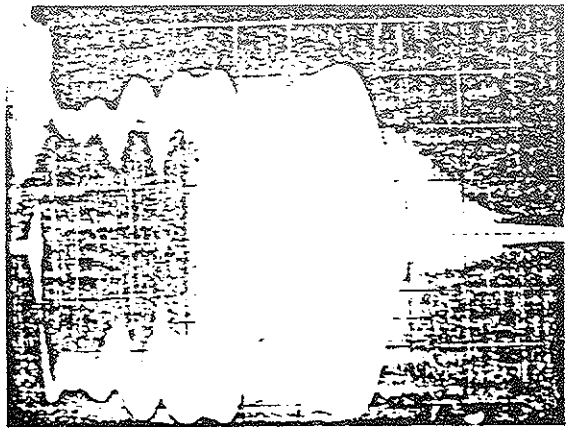

CIRCULATING CURRENT IN HIGH POWER ANTENNA

the circulating current through the hoop shows a small increase. The effect on I_{circ} is indeed small (the vertical gain has been turned up significantly, and a large negative offset placed on the signal). Although the effect is small, it does indeed indicate resonant coupling between the antenna and the resonance.

With the new antenna, this phenomenon is much easier to measure. Not only is the antenna Faraday shielded, but its parallel impedance is also a factor of 5 larger than that for the hoops. In Figure 5.8 (b) we have shown again a probe signal near the resonance peak, and at the bottom the circulating current through the antenna. The resonant loading effect is more pronounced, and a series of resonant loading peaks can be observed.

Alternatively, if one has a steady-state plasma, then the drive frequency could be swept through some range of values in which the frequency matches some given mode which the antenna can drive. One would thus see resonant loading as a function of the frequency. Although this is the better method for controlled comparisons with theoretical loading calculations, it requires a reasonably steady-state plasma, at least for the duration of the sweep. It is not adequate for correlating source loading with resonance profiles, since sweeping can only be done at low power levels, at which one cannot see the resonance above the background plasma noise.

A fundamental question for SARH concerns the optimal orientation of the antenna rf currents with respect to the equilibrium magnetic field direction. As we discussed earlier, it would seem from ideal MHD theory, that the best antenna is a helix which matches the pitch of the mode one is trying to drive. This implies antenna currents parallel to the equilibrium field, thus producing a perturbation field which is perpendicular to the equilibrium field, as is the case with a shear wave.

Unfortunately, it may not be quite this simple. If the antenna currents are parallel to the field, then the induced $\partial \underline{A}/\partial t$ will also be in the equilibrium field direction. Plasma electrons near the surface of the antenna are free to respond to this induced electric field by flowing along the field line. This electron response could effectively shield out the oscillating magnetic field from the interior of the plasma. If that happens, power from the antenna will be dissipated in the region around the antenna. Note that this occurs whether or not the antenna is Faraday shielded, since the $\partial \underline{A}/\partial t$ field is unaffected by the Faraday shield. The effect does not have to be 100% to be important but only enough to lower the efficiency of the system to an unacceptably low value to allow its use in a reactor.

The TCA tokamak[3] has taken the opposite approach to the antenna question by orienting their antenna currents in the

poloidal direction. The rf currents then produce a modulation of the plasma surface due to the magnetic pressure from the oscillating b_ℓ of the wave. Through the coupling between different components of the wave fluid velocity and wave magnetic fields this pressure modulation mode converts to the kinetic Alfvén wave at the resonant surface. Although this method appears at first glance to be a weaker coupling than with a helical antenna, it does avoid the problem of plasma electron shielding of the $\partial \underline{A}/\partial t$ field, since the electrons are tied to field lines and cannot easily respond in the perpendicular direction. The method does seem to have some validity as witnessed by their recently published heating results[4]. However, it still remains to determine what is the most effective coupling scheme, and this will be studied in future experiments on Tokapole II.

We have made some initial measurements to test this idea on Tokapole II. In Figure 5-9 we show the loading (in terms of equivalent series resistance) of the new antenna vs. angular orientation of the antenna. Although there is an asymmetry in the plot, not understood yet, it is clear that a peak in loading occurs for an orientation in which the antenna currents are parallel to the field lines which lie immediately above the antenna. Furthermore, this increased loading does not seem to correlate with any increased resonance amplitude, since there were only small differences in the resonance profiles vs.

Fig. 5-9: Series plasma impedance versus rotational angle of high power antenna. In circuit model of antenna, r_o is series impedance of antenna while r_p is equivalent series impedance of plasma coupled by antenna.

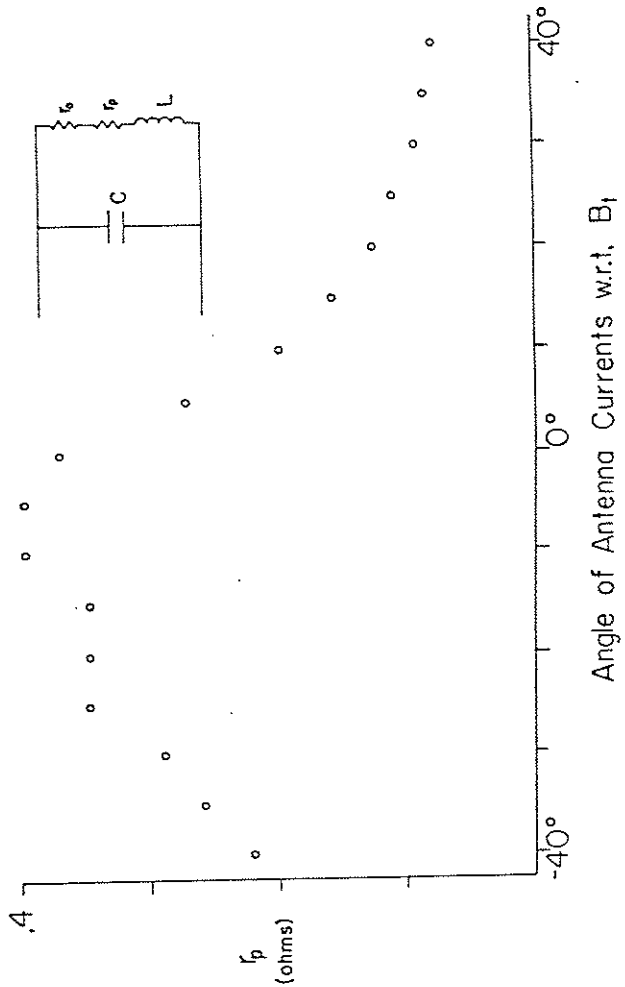

orientation. We believe this may be evidence of $\partial \underline{A}/\partial t$ loading, but it clearly needs more work to be understood completely. We also examined a gun injected, octupole plasma for comparison and found virtually no loading. The rf currents were still in the toroidal direction, but there was no toroidal field present. This is consistent with the above argument concerning loading of $\partial \underline{A}/\partial t$.

Since the present Alfvén antenna does not allow a rotation of more than ±15 deg with respect to the toroidal direction when fully inserted, a new antenna is being designed which can rotate a full ±90 deg[5]. This will allow a good comparison between different antenna orientations in the same device.

5.G. Global structure of resonances generated by new antenna

The most significant observation yet made with the new antenna is that it produces clearly observable resonances at locations far from the antenna. Figure 5-10 shows a resonance measured 90° toroidally around from the antenna location. The vacuum field strength of the antenna at this location is negligibly small. However, when the rf is fired during a plasma discharge we see a very strong resonance which is comparable (~1/2) in strength to those measured immediately above the antenna. The resonance is clearly not being locally excited, but is part of a global resonance structure which is being locally driven immediately above the antenna. Of course,

Fig. 5-10: Radial profile of poloidal wave magnetic field measured 90° around toroidally from high power antenna location.

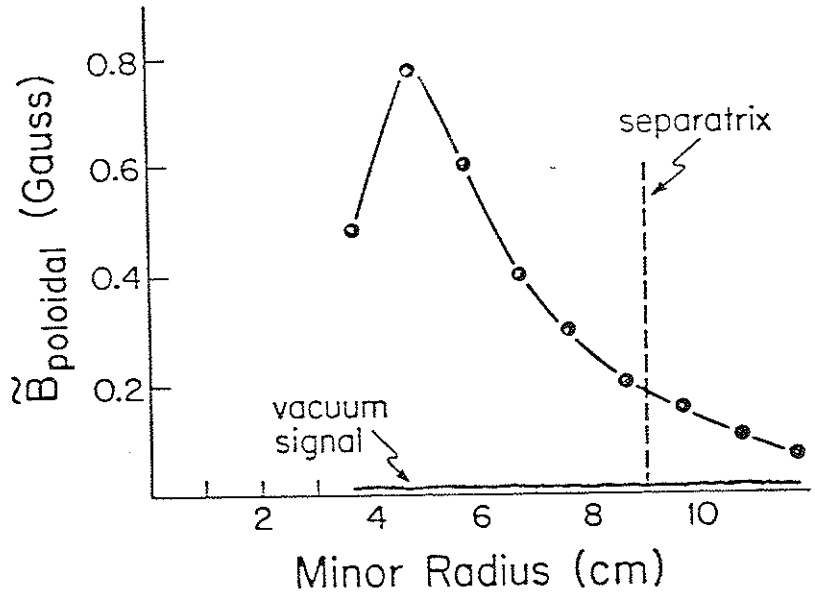

this is just what is expected for the shear Alfvén mode, and this observation appears to be confirmation of this.

This has implications for the future heating experiment, in that even the "point-source" excitation from only one antenna can couple very effectively to the plasma modes. This was always uncertain beforehand, since the hoop antenna had a global structure, and there was no way of driving only a small section at a time to test it. We expect that the other antennas, when added, will provide an even stronger coupling, and that heating should be possible.

5.H. Radial Location

So far it has been shown that all measured properties of the resonances agree with the expected characteristics of a shear Alfvén resonance. What we have now to show is that the resonance occurs at the proper radial location. This is also the most difficult feature of the resonance to compare with theory.

There were two reasons for this difficulty. 1) A 2-D calculation must be performed which takes into account toroidicity and non-circularity of the plasma cross-section. This is especially true for Tokapole II with its squarish cross-section. This must ultimately be done numerically and

has been done by Kieras[6]. 2) In order for this code to make useful predictions, it requires input plasma profiles that accurately reflect those profiles encountered in the experiment. Since good plasma profile data are lacking for Tokapole II, these profiles must be inferred from those measurements which can be made. Planned upgrades and proposed new diagnostics may alleviate this deficiency. (See Chapter 7)

It is the purpose of this Section to analyze a particular resonance for which good mode structure data exists, and demonstrate that very reasonable assumptions concerning the inferred plasma profiles, which are also consistent with global plasma parameters, leads to very good agreement between the measured location of the resonance and the location predicted by theory.

5.H.1. Mode structure data

The resonance data to be discussed are shown in Figure 5-11. In this figure we have plotted the radial profile of the poloidal wave magnetic field. There are three separate profiles. The solid curve is a profile obtained with a probe through the $\phi=60^{\circ}$, $\theta=0^{\circ}$ probe port, The dot-dash curve through the $\phi=90^{\circ}$, $\theta=0^{\circ}$ probe port, and the dashed curve through the $\phi=90^{\circ}$, $\theta=90^{\circ}$ probe port, where ϕ and θ refer to toroidal and poloidal azimuths respectively. In each case the profile was obtained with the stainless steel probe tube tip at the fixed

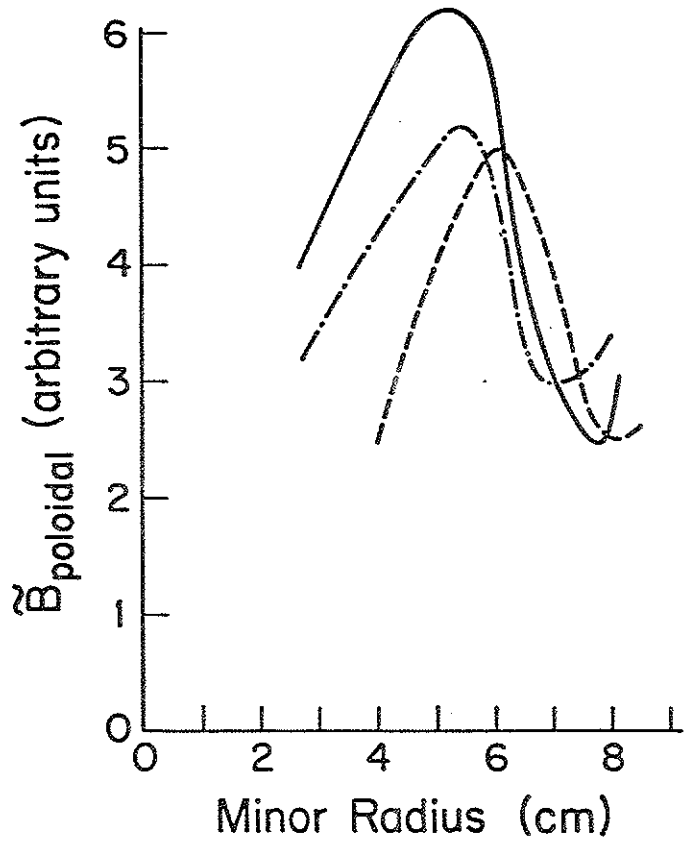

Fig. 5-11: Poloidal wave magnetic field profiles measured along three different chords specified in text. This mode has a measured symmetry of (m,n) = (1,-2). Resonance location along mid-plane is at minor radius of 5.5 cm.

location of 4.0 cm from the axis of the machine where it was left for a series of plasma shots. The single pick-up coil was moved along the axis of the probe tube to a different radial location for each shot. Other probe details have been discussed more fully in Section 4.C and in Reference 7 and will not be repeated here.

In order to match these data with theory, it is necessary to determine its mode identity. This requires a measurement of the difference in phase of the wave magentic field between different toroidal and poloidal locations. Unfortunately, this seemingly simple measurement has turned out to be one of the most difficult attempted in this experiment. Ideally, the difference in phase between two magnetic probes at various toroidal and poloidal azimuthal locations would be sufficient to determine the mode structure. This is not straightforward however, since two probes severely perturb the plasma, and because there were difficulties in obtaining noise free signals from two separated probes due to ground loops at the time these phase measurements were attempted.

A second technique is to use a single probe, measuring its difference in phase with respect to some arbitrary signal that is phase locked to the wave. By making phase measurements at several different locations with respect to this phase reference, one can then readily determine the phase difference between the two positions in the resonance. This reduces the

probe perturbations to that of a single probe. The phase measurement is performed using a dual beam oscilloscope.

The most obvious and appropriate choice for such a phase reference is the circulating rf current through one of the rings. The upper outer ring was used for this case. Obviously this technique only works if there is a stable phase lock between the measured signal and the phase reference from shot to shot. Although many attempts were made to measure mode structures, and many resonances have been observed with various ring antenna configurations, we have been successful in obtaining good mode structure data for only the single case presented here. For this case, excellent phase lock was obtained with the phase reference, as determined by noting that the phase was constant over a large number of plasma discharges. All other attempts were faced with apparently randomly occurring phases which prevented obtaining mode structure data for those resonances. It is not presently understood why this occurs, although there is a very strong suspicion that randomly occurring, plasma generated, rf noise is large enough to cause significant phase shift in the relatively small wave magnetic field of the resonances generated by the ring antenna. Other possibilities are that normal variations in plasma parameters on a time scale of tens of microseconds may have been affecting the resonance structure enough to cause variations. For the data presented here, the

plasma generated noise was sufficiently low to avoid this problem.

Since the measurement technique can only measure phase during one or two cycles of the wave (1-2 μsec), a time history of the phase could never be obtained. A phase detector has recently been constructed and is being tested in conjunction with the new antenna. This will allow continuous phase measurement during the entire rf pulse, rather than at a single instant in time.

Using this measurement technique, the following phases were measured. The phase difference between the (ϕ=60°, θ=0°) and the (ϕ=90°, θ=0°) probe ports on resonance was 60 degrees. Since the toroidal separation is 30 degrees, this implies a toroidal mode number of n=2. The measured phase difference between the (ϕ=90°, θ=0°) port and (ϕ=90°, θ=90°) port on resonance was 90 degrees, indicating a poloidal mode number of 1. From the fourier analysis of the ring antenna it is highly unlikely that the mode numbers are anything other than the lowest mode possible . The best choice for the mode is then $|n|=2$, $|m|=1$.

The global plasma discharge characteristics, with probe inserted, is indicated by the Tokapole II program output of Figure 5-12. This program generates the time evolution of various plasma parameters which have been obtained by a digital data acquisition system[8]. The generic type of discharge is the

Fig. 5-12. Tokapole program output showing discharge characteristics for data of Figure 5-11.

338
MAX IP = 22.8 AT 2100 US
AMP SECONDS = 46.1
TE = 39.7 NE = 1.3 E12
A = 11. Q = 1.5
TAU = 36

TIME	IP	JSAT	BT	VPG	IHOOP
200	0	6	4042	52	39
400	0	9	4142	50	82
600	4	135	4160	48	120
800	11	370	4257	45	153
1000	12	486	4296	42	186
1200	16	539	4316	38	215
1400	19	407	4414	34	240
1600	20	375	4453	30	263
1800	21	449	4511	25	281
2000	23	555	4492	20	296
2200	22	582	4550	16	307
2400	21	562	4589	11	315
2600	19	545	4570	6	320
2800	12	550	4570	2	324
3000	14	472	4570	0	321
3200	8	361	4570	0	321
3400	5	377	4570	0	320
3600	3	320	4609	0	319
3800	1	209	4609	3	319
4000	1	142	4570	4	319
4200	1	117	4589	4	319
4400	0	92	4531	3	319
4600	0	76	4511	2	318
4800	1	64	4472	1	316
5000	0	50	4414	1	314

kind represented by the waveforms of Figure 4-6a. The lower and upper scrape-off plates are extended to their furthest inward extent, so that their inner edges are about 2.0 cm outside the separatrix. This implies that the plasma current measurement yields a more accurate measurement of the current actually flowing within the central current channel.

The rf pulse of approximately 1 msec duration is triggered at 1.7 msec after the ohmic heating trigger. The circulating current through the upper outer hoop was ~20 A zero-to-peak with plasma present. The frequency was 1.16 MHz. The rf trigger time was chosen so that during the rf pulse the plasma parameters are changing least rapidly, allowing an approximation to a steady state.

5.H.2. Comparison with theory

In comparing these data with the predicted resonant location there are two points to consider. Tataronis et al.[9] have shown that even though the Alfvén velocity is not constant on a flux surface, the resonance condition is still satisfied on a flux surface. That is, the eigenvalues ω^2 are flux surface quantities. We should thus expect to observe the resonance lying on a flux surface and not skewing off the surface as the field lines wrap around the torus. This is the first point. The second point is to determine whether the resonance occurs on the correct flux surface.

The global discharge parameters used as input to the equilibrium code are the following.

B_t = 4500 Gauss

I_p = 24 kA

Total flux = 0.065

current peaking parameter = 1.80

The equilibrium code assumes zero plasma current outside the separatrix. This is a bad assumption for normal discharges where as much as 30% of the total plasma current can flow outside the separatrix. However, when discharges are run with the baffles inserted, as is the case here, it becomes a much better approximation, since there is then only a very small amount of plasma current outside the separatrix. A new equilibrium code developed by Uchimoto[10] which allows plasma current outside the separatrix, coupled with Rogowski coil measurements of the plasma current density in the scrape-off region, may significantly improve the match between experimental and theoretical equilibria.

A total flux of 0.065 is chosen to match the total measured hoop current of 288 kA. The current peaking parameter, β, is a free parameter of the equilibrium code[11] which specifies how peaked the plasma current profile should be. It is defined by the expression

$$f(\phi) = R_o B_o[1 + g_p \phi_r^{\beta}]$$

where $\phi_r = (\phi - \phi_1)/(\phi_m - \phi_1)$, ϕ_m is the flux value of the magnetic axis, g_p is a parameter adjusted during each iteration to maintain constant total current, and $f = RB_\phi$. β is chosen to match experimental data.

Recent experimental work by Osborne and Brickhouse[12] have shown that a peaking parameter value in the vicinity of 2.0 is appropriate in order to match the inversion point in sawtooth data obtained from SXR diagnostics with the q=1 surface. Related SXR data shows that the discharge axis lies 2.0±0.5 cm outwards in major radius from the center of the vacuum vessel. A peaking parameter of 1.10 generates a theoretical equilibrium whose magnetic axis lies at the center of the machine, whereas a value of 1.8 produces the required outward shift of roughly 2.0 cm.

The theoretical flux plot for this discharge is shown in Figure 5-13. The magnetic axis lies 1.75±1.0 cm outwards from the machine center. The flux surface on which the resonance lies along the midplane scans has been darkened for clarity. Note that the flux surfaces have a slight vertical elongation which means that the resonance measured along the vertical chord would be expected to lie at a slightly larger minor radius.

Returning to Figure 5-11, we observe that both the

Fig. 5-13: Theoretical poloidal magnetic flux plot for discharge.

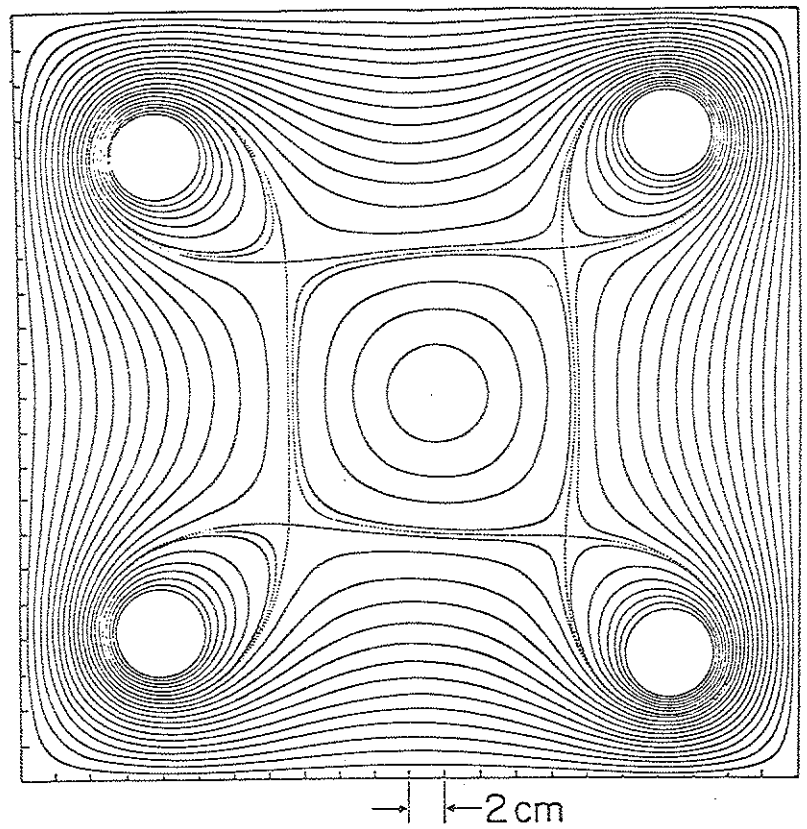

resonance profiles taken along the horizontal chords peak at the same radius while the profile along the vertical chord peaks about 0.5 cm further out. Note that these data are plotted with respect to the magnetic axis location of Figure 5-13 and not with respect to the center of the vacuum vessel. Although individual measurement errors relative to the machine center are ~±0.25 cm, both the vertical and horizontal position of the magnetic axis have errors of roughly ±1.0 cm, causing the systematic error to dominate. Within the accuracy of these measurements, the resonant peaks do indeed lie on a flux surface.

To determine whether the resonance lies on the correct flux surface we have used this equilibrium to provide the input for the frequency spectrum code[6]. This code also requires a mass density profile to be specified separately within the code itself. We have used gaussian profiles since these provide a good match with measurements of the line average density (from the microwave interferometer[13]) and with edge density measurements via Langmuir probes[14]. Since this is a mass density profile, care must be taken to include the contribution to the total mass due to impurities. Using the impurity concentrations of oxygen, copper and aluminum estimated by Brickhouse[15], we have determined the total mass density to be 1.5-1.8 larger than that due to a purely hydrogenic plasma with

the same electron density. The density profile had a peak equivalent proton number density of 1.0×10^{13} cm^{-3} and a half width of 5.0 cm.

The resulting theoretical Alfvén frequency spectrum (continuum) is shown in Figure 5-14 for the four lowest modes. [Some previous attempts to match this data with theory[16] used current profiles that were too flat (corresponding to a peaking parameter of 1.10) and also did not take into account the contribution to the mass density due to impurities. These inaccuracies have been corrected here.] For the (1,-2) mode, a resonance at 1.16 MHz is predicted to occur at 5.0 cm along the horizontal mid-plane. This agrees very well with the observed location of the (1,-2) mode in Figure 5-11, where the resonance peaks at ~5.25±1.25 cm. For variations of the density profile, toroidal magnetic field and plasma current profile within the limits of their measurements, the location of the (1,-2) mode is predicted to occur within ±2.00 cm of its measured location.

The fact that the (1,-2) mode is the most likely mode predicted to occur in a region where a (1,-2) mode is experimentally observed seems to be strong evidence in favor of agreement between theory and experiment.

Fig. 5-14: Theoretical continuum Alfven spectrum for discharge predicts (m,n) = (1,-2) mode resonance location at 1.16 MHz at a minor radius of 5.0 cm along mid-plane.

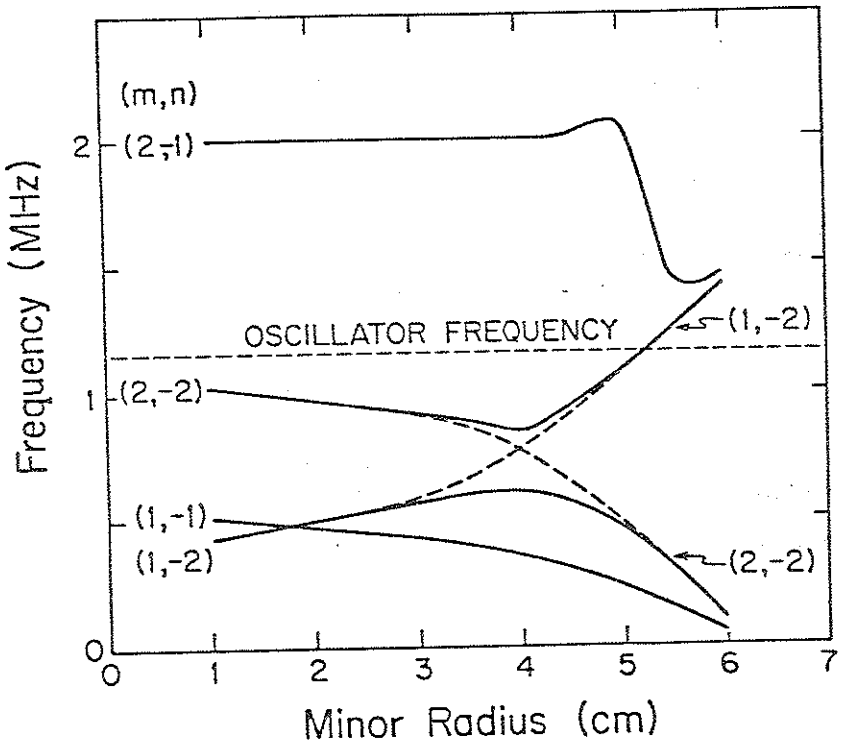

REFERENCES - CHAPTER 5

1. A. Hasegawa and L. Chen, Phys. Fluids 19, 1924 (1976).

2. C.M. Fortgang, Ph.D. Thesis, University of Wisconsin (1983).

3. A.D. Chettham, A. Heym, et al., CRPP Internal Report LRP 162/80, Lausanne (1980).

4. R. Behn, A. de Chambrier, et al., CRPP Internal Report LRP 232/83, Lausanne (1983).

5. D. Kortbawi, F.D. Witherspoon, J.C. Sprott, and S.C. Prager, Bull. Am. Phys. Soc. 28, 1086 (1983).

6. C.E. Kieras, Ph.D. Thesis, University of Wisconsin (1982).

7. F.D. Witherspoon, University of Wisconsin PLP 921 (1984).

8. J.C. Sprott, University of Wisconsin PLP 889 (1983).

9. J.A. Tataronis, J.N. Talmadge, and J.L. Shohet, Proc. 3rd Topical Conf. on RF Plasma Heating, (Pasadena, 1978); also Comments Plasma Phys. Controlled Fusion 7, 29 (1982).

10. E. Uchimoto, J.D. Callen, L. Garcia, and B.A. Carreras, Sherwood Theory Conference, paper 1Q19 (1984).

11. M.W. Phillips, University of Wisconsin PLP 765 (1978).

12. T.H. Osborne and N.S. Brickhouse, University of Wisconsin PLP 908 (1983).

13. T.J. Kruzel, University of Wisconsin PLP 831 (1980).

14. T.D. Rempel and G.A. Emmert, University of Wisconsin PLP 894 (1983).

15. N.S. Brickhouse, Ph.D. Thesis, University of Wisconsin (1984).

16. S.C. Prager, F.D. Witherspoon, C.E. Kieras, D. Kortbawi, J.C. Sprott, and J.A. Tataronis, in 5th Topical Conf. on RF Heating in Plasmas, (Madison, 1983).

CHAPTER 6

CONCLUSIONS AND COMMENTS

The main experimental conclusions of this thesis are summarized as follows:

1) The observed resonances have wave fields which are polarized perpendicular to the equilibrium magnetic field, as required for the shear Alfvén wave.

2) The measured radial location is in agreement with the predictions of a 2-D calculation which takes into account both toroidicity and non-circularity of the plasma cross-section.

3) The resonance lies on a flux surface as predicted analytically.

4) The radial width is in good agreement with rough calculations based on ohmic dissipation of the wave resonance energy, but is a factor of four smaller than the estimated width due to electron Landau damping. This seems to be consistent with the intermediate collisionality regime of the electrons in these discharges.

5) The rise time of the wave fields to a saturated value is consistent with the upper bound limits that can be placed on the measured risetime due to finite oscillator risetime effects.

6) The resonant enhancement factor of the wave fields over the corresponding vacuum wave fields is in rough agreement with predicted enhancement factors for the divertor ring antenna system, and is consistent with expectations for the new antenna.

7) Correlation between the wave fields and observed resonant loading effects are consistent with expected qualitative loading behaviour, but more work is necessary to quantify this in the future with the new antenna.

8) Results from the new antenna indicate that global mode structures are readily driven by local excitation, i.e. resonances have been observed at toroidal locations which are distant from the vacuum antenna fields, indicating toroidal wave propagation from the antenna.

At this point, a few remarks are in order concerning what else the observed wave enhancement might be. Since the wave is two orders of magnitude larger than the drift wave frequency

(ω^*~10 kHz), the mode is not likely to be a drift wave or unstable resistive or ideal MHD mode, all of which oscillate at about ω^*. Since the wave frequency is much less than the ion cyclotron frequency ($\omega=\omega_{ci}/6$), finite ω/ω_{ci} effects should not play a role. Also, since the mode is radially localized, it is not likely to be a driven stable discrete global kink mode as observed on Pretext[1] and inferred on TCA[2].

Since all measured properties of the resonances are in good agreement with predictions, and since there does not appear to be any other known phenomenon which can explain the results, we are led to the conclusion that these observations constitute an experimental identification of the shear Alfvén resonance in a tokamak.

This experiment does not end here however; on the contrary, this is just the beginning. We have taken the first steps towards an experimental investigation of a new rf heating technique. We have shown that the resonance does exist in a tokamak with properties that are in good agreement with theory. It is now time to proceed to the next stages of the experiment.

There are two primary goals for future SARH research on Tokapole II, both of which are closely related. The first is to continue studies of the resonances, refining and broadening the scope of the measurements in order to strengthen the

identification and provide more detailed knowledge of the resonances. It is interesting to note that, although ion cyclotron resonance was identified in tokamaks long ago, productive and necessary studies of the wave properties (with mode conversion, minority ions, different antenna configurations, etc.) continue to this day in many tokamaks. A similar process can also be expected to occur for SARH in the coming years. The second goal is to perform a high power heating experiment and study the heating process in detail.

One fundamental prerequisite for making progress towards these goals is to obtain better plasma profile information than is currently available. We have shown in this thesis that reasonable assumptions concerning the profiles lead to good agreement with theory. However, if more definitive comparisons with theory are to be made, it will be necessary to use more accurate models for the plasma profiles. What is most needed are profiles of density and current. Planned improvements in the SXR array should be of considerable aid in determining the location of the q=1 surface and the T_e profile. These in turn will aid in modelling the current profile. Rogowski-coil measurements of the plasma current density in the divertor scrape-off region, coupled with an equilibrium code recently developed by Uchimoto[3] which allows for plasma current outside the separatrix, could also go a long way toward constructing an equilibrium that more closely matches experiment. A

multi-chord microwave interferometer would help to pin down the density profile, since it is not possible to insert Langmuir probes past the separatrix.

Along this same line is the need to more accurately determine the perturbations to the plasma discharge by magnetic probes which have been inserted past the separatrix. Although the recently introduced boron-nitride sheathed magnetic probes seem to have solved the problem of probe destruction, they still cause significant perturbations to the discharge, albeit somewhat less than the smaller stainless steel probes used previously. In addition to this, a study of the effects of runaway electrons on the discharge, and in particular their interaction with probes, seems to be warranted.

As far as measurements of the resonance properties is concerned, the single most important improvement in these studies will be the utilization of a vastly superior launching structure. The new antennas will make it possible to perform much more controlled experiments than were ever possible with the rings. The coupling to helical modes will be stronger than the rings could achieve, and considerably easier to interpret. The vastly increased power handling capability of the rf system will allow the wave field measurements, especially the phase measurements, to be performed more reliably since background plasma noise will be a small perturbation on the wave signal which has not been the case with the rings.

Coupling to specific modes with virtually zero coupling to other closely lying modes appears to be possible with the new antenna. This has never been possible with the rings, and complicates things considerably. With the good mode control that is expected from the new antennas, and with the ability to easily and quickly change the frequency of the rf system, it should be possible to do the definitive frequency change experiment, in which the frequency of the rf system is varied while maintaining all plasma parameters constant. This should shift the radial location of the resonance in one direction or the other depending on the specific mode being observed (see Figure 5-14). If sufficient profile information is available, including good mode structure data, it should be possible to predict which direction the resonance will shift and by what amount. Such a measurement would provide further confirmation of the resonance identification. Attempts to do this experiment with the divertor ring antenna have been consistently frustrated by hardware limitations. It is suggested that some emphasis be placed on this experiment in the future in conjunction with mode structure studies with the new antenna system. It should be emphasized that this experiment is of only marginal value unless good mode structure data can be obtained via phase measurements.

Along the same lines as the above experiment is another interesting feature of the theory, i.e. the prediction of

frequency gaps in the spectrum. If such gaps do indeed exist, it might be possible to detect them, but only if coupling to a specific mode can be demonstrated with the antennas. As the frequency is lowered (raised) for a particular mode, it could be possible to observe the mode's disappearance and reappearance again at a lower (higher) frequency, but with its poloidal mode number differing by one. This would be a very impressive experimental achievement and would provide even further confirmation of the theory.

A primary function of the new antenna system is, of course, to perform heating studies. The ability to heat a plasma in this frequency range has been recently demonstrated on the TCA tokamak at Lausanne[2]. This result effectively certifies SARH as a technique worthy of intensive and broadbased experimentation. Since Tokapole II has an ohmic heating power of 50-100 kW, coupling even 10 kW to the plasma from the antenna should have observable effects. With 1 MW eventually to be available with four antennas installed, coupling a few tens of kilowatts of power should be achievable. This is sufficient for examining the various aspects of heating such as antenna design and correlation studies between the resonance structures and loading of the antenna. Attainment of record temperatures is not a goal and should be left to tokamaks which have the required high plasma currents. Instead, these experiments should concentrate on studying the

physics of the heating process. Some key physics issues to be addressed are the following:

1) What is the heating mechanism in different collisionality regimes, and which species get heated?

2) What is the optimal antenna current orientation with respect to the equilibrium field? Determining the answer to this question on Tokapole II could be of enormous value in the design of future high power SARH experiments on large tokamak devices. This particular question should receive a great deal of attention since Tokapole II seems to be an ideal device to test this in, because of the large divertor scrape-off region in which to place antennas.

3) Do observed resonances correlate with antenna loading, and if so do they agree with theoretical calculations? This will require development of a 2-D code to calculate loading numerically in the Tokapole II geometry somewhat similar to the frequency spectrum code developed by Kieras[4] to predict the resonance location.

4) If frequency gaps in the spectrum can be experimentally shown to exist, what will be their effect on heating? Will they simply indicate regions in which no heating can occur, or will more subtle effects be discovered?

5) What region of the plasma will be heated? Will it

really occur on a flux surface, or will it be spread over a larger region?

6) What is the heating efficiency for various plasma conditions and antenna configurations? Will the low beta of Tokapole II prevent core heating? Can core heating be turned on or off simply by raising or lowering beta past the critical value of m_e/m_i? Can the kinetic Alfvén wave be excited in the Tokapole II device.

7) What happens to the confinement time as the rf heating power levels are raised? Will there be enhanced radial transport of plasma?

REFERENCES - CHAPTER 6

1. T.E. Evans, et al.; M.E. Oakes, et al.; and R.D. Bengtson, et al., Bull. Am. Phys. Soc. 28, 1085 (1983); R.D. Bengtson, et al., in 5th Topical Conf. on RF Heating in Plasmas, (Madison, 1983).

2. R. Behn, A. de Chambrier, et al., CRPP Internal Report LRP 232/83, Lausanne (1983).

3. E. Uchimoto, J.D. Callen, L. García, and B.A. Carreras, Sherwood Theory Conference, paper 1Q19 (1984).

4. C.E. Kieras, Ph.D. Thesis, University of Wisconsin (1982).